ISSN 0801-9940 No. 03
July 2013

EFFICIENT ANALYTICAL SOLUTIONS FOR HEATED, PRESSURIZED MULTI-LAYER CYLINDERS

by

Knut Vedeld and Håvar A. Sollund

RESEARCH REPORT
IN MECHANICS

UNIVERSITY OF OSLO
DEPARTMENT OF MATHEMATICS
MECHANICS DIVISION

UNIVERSITETET I OSLO
MATEMATISK INSTITUTT
AVDELING FOR MEKANIKK

DEPT. OF MATH., UNIVERSITY OF OSLO
RESEARCH REPORT IN MECHANICS, No. 3
ISSN 0801-9940 July 2013

EFFICIENT ANALYTICAL SOLUTIONS FOR HEATED, PRESSURIZED MULTI-LAYER CYLINDERS

by

Knut Vedeld and Håvar A. Sollund

Mechanics Division, Department of Mathematics
University of Oslo, Norway

Abstract: Two independent sets of analytical solutions, one based on matrix inversion and one based on iteration, are derived for the displacement field and corresponding stress state in multi-layer cylinders subjected to pressure and thermal loading. Solutions are developed for cylinders that are axially free with no friction between layers (plane stress), for cylinders that are fully restrained axially (plane strain) and for axially loaded and spring-mounted cylinders, assuming that the combined two-layer cross-section remains plane after deformation (generalized plane strain). The analytical solutions are verified by means of detailed three-dimensional finite element analyses and comparisons between the two independent analytical solutions, which are easily implemented in, and suitable for, engineering applications.

Keywords: Multi-layered cylinder, plane stress, plane strain, generalized plane strain, pressure, temperature, analytical solution, pipelines

TABLE OF CONTENTS

NOMENCLATURE

a_i	Recurrence relation, defined by Eq. (70) [-]
A_i	$= -\hat{E}_i(1-2\nu_i)C_{r1,i}$ [N]
$A_{s,i}$	Steel cross-sectional area for layer i [m^2]
b_i	Recurrence relation, defined by Eqs. (70) (plane stress / plane strain) and (82) (generalized plane strain) [-]
C	General constant (used for strain under generalized plane strain) [-]
$\mathbf{C}[a\ ,\ b]$	Space of continuous functions on the interval $[a\ ,\ b]$
c_i	Recurrence relation, defined by Eq. (87) [-]
C_i	$= \frac{E_i}{1-\nu_i} C_{r2,i}$ (plane stress); $= \hat{E}_i C_{r2,i}$ (plane strain / generalized plane strain) [Pa]
C_{r1}	Displacement coefficient in radial direction [m^2]
$C_{r1,i}$	Displacement coefficient in radial direction for layer i [m^2]
C_{r2}	Displacement coefficient in radial direction [-]
$C_{r2,i}$	Displacement coefficient in radial direction for layer i [-]
C_z	Displacement coefficient in axial direction [m]
$C_{z,i}$	Displacement coefficient in axial direction for layer i [m]
$\mathbf{D}$	Displacement coefficient vector
d_i	Recurrence relation, defined by Eq. (87) [-]
E	Young's modulus [Pa]
$\mathbf{E}_i$	Generalized Young's modulus in layer i [Pa]
E_i	Young's modulus for layer i [Pa]
$\hat{E}$	$= E / ((1 + \nu)(1 – 2\nu))$ [Pa]
$\hat{E}_i$	$= E_i / ((1 + \nu_i)(1 – 2\nu_i))$ [Pa]
i	Layer index [-]
k	Axial spring stiffness [N/m]
K	$= k / 2$ [N/m]
$\mathbf{K}$	Stiffness matrix
$\mathbf{k}_0$	Block matrix component of $\mathbf{K}$, defined by Eqs. (38) and (44).
$\mathbf{k}_i^1$	Block matrix component of $\mathbf{K}$, defined by Eqs. (38) and (44).
$\mathbf{k}_i^2$	Block matrix component of $\mathbf{K}$, defined by Eqs. (38) and (44).
$\mathbf{k}_i^3$	Block matrix component of $\mathbf{K}$, defined by Eq. (53).
$\mathbf{k}_i^4$	Block matrix component of $\mathbf{K}$, defined by Eq. (53).
$\mathbf{k}_n$	Block matrix component of $\mathbf{K}$, defined by Eqs. (38) and (44).
K_z	Component of $\mathbf{K}$ defined by Eq. (51) [N/m]
L	Length of cylinder
n	Total number of layers [-]
N	Applied axial load [N]
P	Axial section force [N]
p_{ext}	External pressure [Pa]
p_{int}	Internal pressure [Pa]
q_0	$= p_{int}$ [Pa]
q_i	Contact pressure between layer i and (i+1) [Pa]
$q^0{}_i$	Contact pressure between layer i and (i+1) for plane strain [Pa]
q_n	$= p_{ext}$ [Pa]
r	Radial coordinate variable [m]
$\mathbf{R}$	Load vector
R_z	Component of $\mathbf{R}$ defined by Eq. (51) [N]
r_0	Inner radius of combined cross-section [m]
r_i	Outer radius of cylinder layer i [m]
r_n	Outer radius of combined cross-section [m]
S_i	$= (\lambda_i - \beta_{i+1})\gamma_{i+1}\gamma_i + (\lambda_{i+1} - \lambda_i)\gamma_i$ [Pa^{-1}]
t_i	Thickness of layer i [m]
T_i	$= \lambda_{i+1} - \beta_i + (\beta_i - \beta_{i+1})\gamma_{i+1}$ [Pa^{-1}]
u_r	Displacement field component in radial direction [m]
$u_{r,i}$	Displacement field component in radial direction for layer i [m]
u_z	Displacement field component in axial direction [m]
$u_{z,b}$	Displacement field component in axial direction for layer i [m]
u_θ	Displacement field component in circumferential direction [m]
$u_{\theta,b}$	Displacement field component in circumferential direction for layer i [m]
x	Cartesian coordinate [m]
y	Cartesian coordinate [m]

z	Cartesian/cylindrical coordinate [m]
z_e	Axial coordinate of cylinder end [m]
α	Temperature expansion coefficient for inner layer [°C^{-1}]
α_i	Temperature expansion coefficient for layer *i* [°C^{-1}]
β_i	$=(1-\nu_i)/E_i$ (plane stress); $=1/\hat{E}_i$ (plane strain / generalized plane strain) [Pa^{-1}]
γ_{i+1}	$=r_i^2/r_{i+1}^2$ [-]
$\gamma_{ij,i}$	Shear strains in layer *i* [-]
ΔT	Change in temperature [°C]
ΔT_i	Change in temperature in layer *i* [°C]
$\varepsilon^0_{ij,i}$, $\boldsymbol{\varepsilon}_{0,\mathrm{i}}$	Tensor of initial strains for layer *i* [-]
ε_{ij} , $\boldsymbol{\varepsilon}$	Strain tensor [-]
$\varepsilon_{ij,i}$, $\boldsymbol{\varepsilon}_i$	Strain tensor for layer *i* [-]
ε_{zz}	$=C_z/L$ (axial strain) [-]
ζ_i	$=\left(d_i-\frac{d_n}{a_n}a_i\right)q_0$ [Pa]
θ	Circumferential coordinate [-]
λ_i	$=-\frac{1}{\hat{E}_i(1-2\nu_i)}$ [Pa^{-1}]
μ_i	$=\varphi_i-\hat{E}_i\nu_i\varepsilon_{zz}$ [Pa]
ν	Poisson's ratio [-]
ν_i	Poisson's ratio for layer *i* [-]
$\sigma^0_{ij,i}$, $\boldsymbol{\sigma}_{0,\mathrm{i}}$	Tensor of initial stresses for layer *i* [Pa]
σ_{ij} , $\boldsymbol{\sigma}$	Stress tensor [Pa]
$\sigma_{ij,i}$, $\boldsymbol{\sigma}_i$	Stress tensor for layer *i* [Pa]
τ_{ij}	Shear stresses [Pa]
φ_i	$=\hat{E}_i\alpha_i\Delta T_i(1+\nu_i)$ [Pa]
ψ_i	$=0$ (plane stress); $=2\nu_i C_i-\varphi_i$ (plane strain / generalized plane strain) [Pa]

1 INTRODUCTION

Cylinders subjected to pressure and temperature have been widely studied, and an analytical solution for the displacement field of a linearly elastic, isotropic hollow cylinder exposed to uniform internal and external pressure was derived by the French mathematician Gabriel Lamé already in 1831 [Lamé and Clapeyron, 1831]. The solution suggested by Lamé is readily adapted for application to shrink-fit problems [Timoshenko, 1958]. Since Lamé's solution gives the full three-dimensional stress state of a pressurized cylinder, the solution is highly useful for design of pressurized thick-walled cylindrical members or disks. However, conventional single-layer pressure vessels are often not suited for operation in extreme environments, with conditions characterized by high pressure and high temperature, and potentially a strongly corrosive fluid content [Zhang et al., 2012]. By increasing the number of cylindrical layers, a larger number of design variables become available to the designer. Naturally, this flexibility facilitates more optimal design for each specific application. Two-layer and multi-layer cylinder designs are therefore often utilized for e.g., pressure vessels [Jahed et al., 2006; Wilson and Skelton, 1968], pipelines [Smith, 2012; Vedeld et al., 2012], piping systems [Marie, 2004; Olsson and Grützner, 1989] and risers [Kloewer et al., 2002].

Another way to overcome the challenges related to extreme operating conditions is to apply advanced materials with tailor-made material properties, such as composites and functionally graded materials (FGMs). FGMs are microscopically inhomogenous materials with mechanical properties that vary smoothly and continuously in one or more spatial directions. The special properties of FGMs are achieved by gradually varying the volume fraction of the constituent materials, typically a mixture of a ceramic and one or more metals [Peng and Li, 2010; Reddy and Chin, 1998]. The FGMs were initially developed to withstand the extreme thermal loading associated with aerospace applications, such as propulsion systems in future space planes, and have commonly been used as thermal barrier materials [Koizumi, 1993; Noda, 1999; Yamanouchi et al., 1990]. Hollow cylindrical vessels and pipes are common structural components for high-temperature or high-pressure applications in nuclear reactors, chemical plants and oil and gas transportation. Therefore, the properties of FGM cylinders have been extensively studied in recent years, focusing on both elastic and elasto-plastic response to pressure loading [Eraslan and Akis, 2006; Shi et al., 2007; Tutuncu and Ozturk, 2001; Xiang et al., 2006], as well as on thermoelastic response [Jabbari et al., 2002; Liew et al., 2002; Ootao and Tanigawa, 2006; Peng and Li, 2010; Reddy and Chin, 1998].

The governing equation for hollow cylinders under axisymmetric loading is an ordinary differential equation with variable coefficients. Such differential equations are possible to solve analytically in certain cases, depending on the functional representation of the material properties [Peng and Li, 2010]. It is common to express the FGM properties of a cylinder as either power functions or exponential functions of the radial coordinate *r*, but other functional relationships have also been studied [Horgan and Chan, 1999; Jabbari et al., 2003; Tutuncu, 2007; Xiang et al., 2006]. The radial displacement field in pressurized FGM cylinders was derived by Xiang et al. [2006], assuming either a linearly graded material, in which the elastic modulus varied linearly in the radial direction while Poisson's ratio was a constant, or an exponentially graded material, in which the elastic stiffness coefficients were assumed to be exponential functions of *r*. In a recent study by Peng and Li [2010], the thermoelastic problem of an FGM hollow cylinder with arbitrary non-homogenous material properties was converted to a Fredholm integral equation, which was solved numerically.

Xiang et al. [2006] did not include thermal stresses in their analysis, but complemented their analytical solution for FGM cylinders by the introduction of a recursive algorithm for the exact elastic analysis of a pressurized multi-layer cylinder with arbitrary number of layers and uniform material properties in each layer. Moreover, it was shown by Xiang et al. [2006] that the multi-layer solutions converged towards the analytical solutions for FGM cylinders as the number of layers was increased. Thus, if the recursive algorithm introduced by Xiang et al. [2006], and later presented also in a paper by Shi et al. [2007], could be extended to include thermal stresses, it would be an attractive method for thermoelastic analysis of FGM cylinders. Based on a similar idea, Liew et al. [2003] developed an analytical model for FGM hollow cylinders subjected to an arbitrary temperature field by dividing the cylinder into a number of homogenous sub-cylinders. However, the hollow cylinder was assumed to be free from pressure loading and only the case of plane strain was considered in the study by Liew et al. [2003].

In the present study, the elastic response of multi-layer hollow cylinders subjected to pressure and temperature will be investigated using two different solution strategies, both of which are based on Lamé's solution for single-layer cylinders. First, the displacement field and stress state of the multi-layer cylinder will be determined from simple and physically transparent equilibrium and kinematic compatibility requirements. This leads to a system of equations, which may be solved by matrix inversion. Thereafter, the recursive algorithms for exact elastic analysis of multi-layer cylinders previously presented by Xiang et al. [2006] and Shi et al. [2007] will be significantly extended to include thermal stresses. The recursive

algorithms of Xiang et al. [2006] and Shi et al. [2007] represent solutions to a non-linear difference equation. Shi et al. [2007] and Xiang et al. [2006] indicate the accuracy of their solutions by comparing results to specific examples. In the present study, the general solutions to the difference equations derived by Shi et al. [2007] and Xiang et al. [2006] are proven formally by means of induction. Furthermore, the new solutions presented herein, which include thermal stresses and additional considerations for boundary conditions, are also proven formally by induction. The results of the novel recursive algorithm will be compared to results from the matrix-based analytical solution, as well as to results from finite element analyses (FEA). Furthermore, both of the solution methods will be applied to three different axial boundary conditions. These include cylinders that are fully restrained axially, corresponding to a plane strain condition, and two types of conditions for axially free cylinders. Axially unrestrained cylinders are analyzed both for the case of individual layers that are free to slide relative to each other, corresponding to a plane stress condition, and for the case of tightly bonded cylinder layers, corresponding to a generalized plane strain condition. The latter condition is particularly relevant for pipelines and piping systems [Vedeld and Sollund, 2013]. In the previous work by Xiang et al. [2006] and Shi et al. [2007], only plane stress and plane strain conditions were considered.

With regard to pipeline and piping applications, multi-layered cylinder cross-sections are highly common. For instance, due to transportation of highly corrosive fluids, for example well fluids with CO_2 or H_2S content, some offshore pipelines have a liner or clad layer made from a corrosion-resistant alloy. In addition, the pipeline cross-section will consist of the main pipe (commonly termed the linepipe) which is typically made of carbon-manganese (CMn) steel, and various coating layers, such as external corrosion coating, insulation coating, and in some cases weight coating of reinforced concrete [Braestrup et al., 2005; Palmer and King, 2004; Vedeld et al., 2012]. Despite the fact that pipeline cross-sections tend to be multi-layered, the leading design codes such as DNV-OS-F101 [2012] and ASME B31.8 [2003], give detailed capacity criteria only for monolithic pipe cross-sections, while additional layers such as liner, cladding or concrete coating are conservatively disregarded in terms of their contribution to structural strength. Furthermore, the potential effects that coating layers may have on important design parameters such as the effective axial force [Sparks, 1984; Fyrileiv and Collberg, 2005] are not considered. The exact three-dimensional analytical solutions that will be presented and thoroughly validated in the present study are, as well as being of theoretical interest in a classical discipline of solid mechanics, easily implemented in e.g., spreadsheet-based engineering tools and thus suitable for practical design contexts.

2 PROBLEM DEFINITION

2.1 A Priori Assumptions

(i) The materials in the cylinder layers are assumed to be linearly elastic, homogenous and isotropic.

(ii) Initial stresses and strains are disregarded.

(iii) Bending effects are not considered. The cylinders are assumed to be perfectly straight, and the influence of curvature on the calculation of stresses due to heat and pressure is not considered.

(iv) Small displacements are assumed. Thus, the load is applied on the initial geometry, and changes in internal or external diameter and changes in layer wall thickness due to the application of loading are not accounted for.

(v) The applied internal and external pressures are radial and uniformly distributed along the inner and outer surfaces of the cylinder, i.e., the pressures are treated as hydrostatic.

(vi) Heat is assumed to result in a uniform temperature distribution within each cylinder layer.

(vii) Different cylinder layers may have different material properties, including elastic moduli, Poisson's ratios and temperature expansion coefficients.

(viii) For plane stress conditions, it is assumed that the cylinder layers are free to slide relative to each other (without friction) in the axial direction. End effects are disregarded.

(ix) Sections that are plane and perpendicular to the cylinder axis prior to deformation are assumed to remain plane and perpendicular to the cylinder axis after deformation for plane strain and generalized plane strain conditions.

2.2 Coordinate system

The standard cylindrical coordinate system defined in Figure 1 is adopted in the present study.

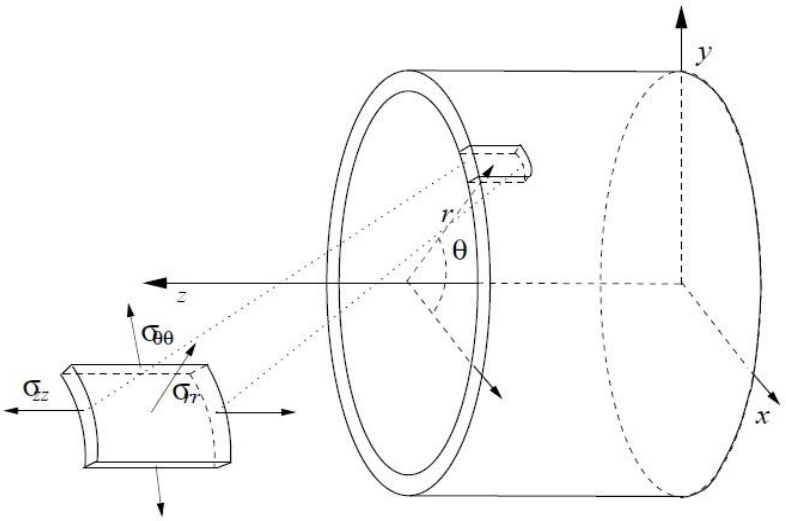

Figure 1 – Cylindrical coordinate system and stress nomenclature.

In the figure, x, y and z are the standard Cartesian coordinates, r is the radial coordinate, θ is the angle between the position vector and the x-axis, σ_{rr} is the radial stress, σ_{zz} is the axial stress and $\sigma_{\theta\theta}$ is the hoop stress.

2.3 Boundary conditions

In the present study, multi-layer cylinders subjected to heat and internal and external pressure will be investigated. An illustration of the problem is shown in Figure 2.

In Figure 2, p_{ext} is the external pressure, p_{int} is the internal pressure, r_0 is the internal radius of the multi-layer cylinder, and r_i is the outer radius of the i-th cylinder layer. E_i is the Young's modulus, v_i the Poisson's ratio and α_i the coefficient of thermal expansion in layer i. The temperature change (relative to a common reference temperature T_0 for all the layers) in the i-th layer is ΔT_i, and q_i (not shown in the figure) is the contact pressure between layer i and layer (i+1). At the inner surface the contact pressure q_0 is equal to the internal pressure p_{int} and at the outer surface the contact pressure q_n is equal to the external pressure p_{ext}. All cylinder layers have the same initial length L.

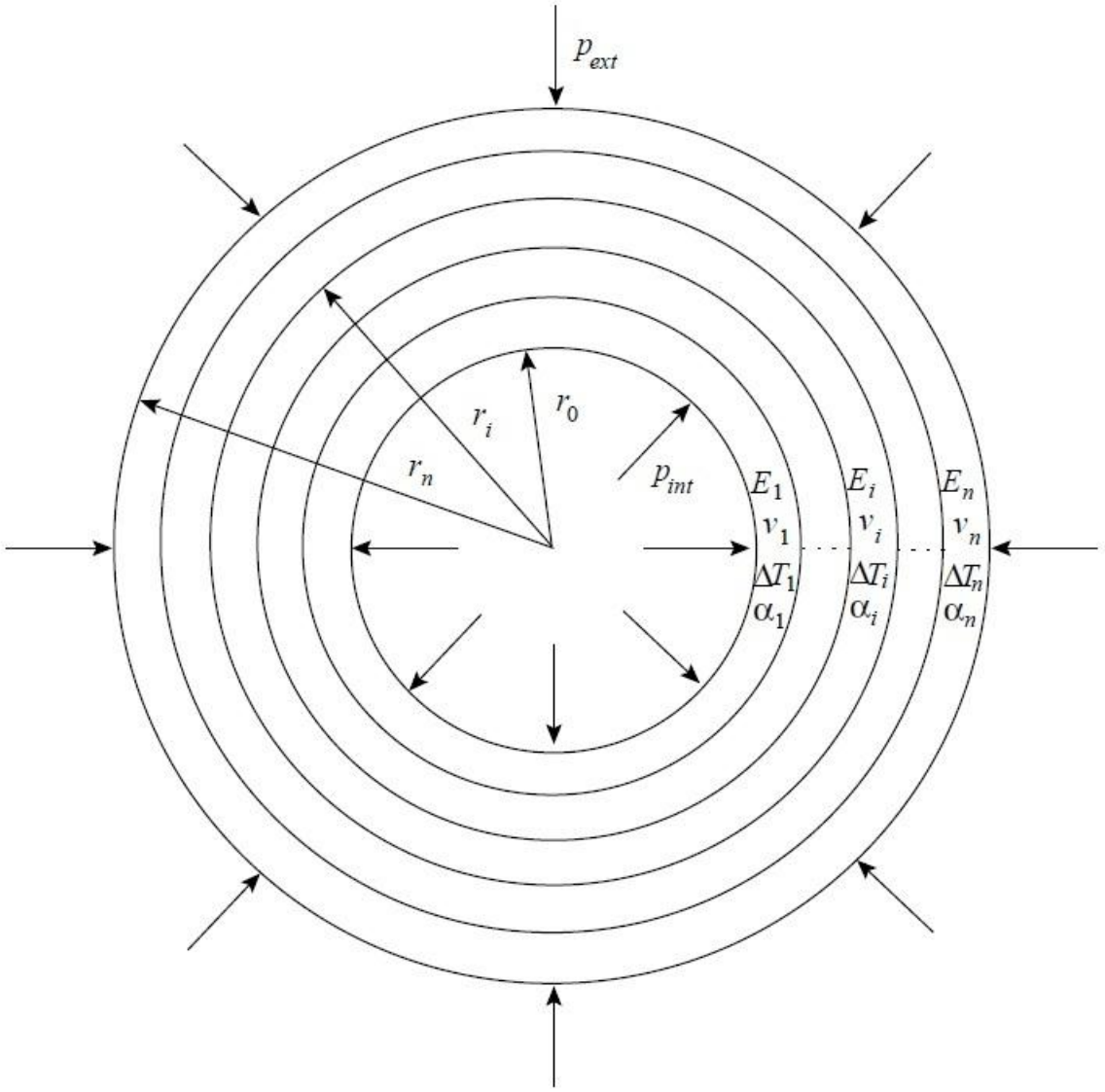

Figure 2 – Multi-layer cylinder with varying material properties E_i, ν_i and α_i in each layer. Temperature changes ΔT_i and radii r_i are also indicated.

On the inner surface, the radial stress must be compressive and equal to the internal pressure, resulting in a static radial boundary condition given by

$$\sigma_{rr,1}(r_0) = -p_{int} \ , \tag{1}$$

where $\sigma_{rr,1}$ is the radial stress in the innermost layer. Similarly, the static radial boundary condition on the outer surface is given by

$$\sigma_{rr,n}(r_n) = -p_{ext} \ , \tag{2}$$

where $\sigma_{rr,n}$ is the radial stress in the outermost layer.

All the cylinders that will be considered have length L and are assumed free to expand or contract radially. With regard to the axial stress and strain state of the multi-layer cylinders, three types of conditions will be presented and studied in the following:

1) Plane stress.
2) Plane strain.
3) Generalized plane strain (with axial loading and spring support).

According to assumption (viii), the cylinder layers are axially free, as well as free to slide relative to each other, under the plane stress condition. The condition may be mathematically represented by

$$\sigma_{zz,i} = 0 \quad \text{for all } i\,, \tag{3}$$

where $\sigma_{zz,i}$ is the stress in axial direction in layer i.

Kinematic boundary conditions and static axial boundary conditions (axial loading) for the two remaining conditions are displayed in Figure 3. In the figure, arrow heads indicate translational constraints and double arrow heads indicate rotational constraints. Each of the cylinders a) and b) may be regarded as representing a segment, or cut-out, of a long pipeline or piping system, which implies that end effects are ignored and that there are no end-caps. The cross-section consists of layers that are axially fixed to each other, either continuously or at regular intervals (assumption (ix) applies).

Cylinder a) in Figure 3 is fully restrained axially. The boundary condition is thus characterized by plane strain, with a mathematical representation defined by

$$\varepsilon_{zz,i} = 0 \quad \text{for all } i\,, \tag{4}$$

where $\varepsilon_{zz,i}$ is the strain in axial direction in layer i. Hence, the axial strain is known, while the axial reaction load is unknown.

For the second boundary condition, illustrated by cylinder b) in the figure, the cylinder is fully restrained at only one end ($z = 0$). At the opposite end ($z = L$), the cylinder may expand axially, but the cross-section must remain plane in accordance with assumption (ix) in Section 2.1. This is visualized in Figure 3 b) by a kinematic coupling, indicated by dashed lines, between a reference point (RP) and the cylinder end surface. Thus, the cylinder is in a state of generalized plane strain, defined by

$$\varepsilon_{zz,i} = C \quad \text{for all } i\,, \tag{5}$$

where C is a non-zero constant. The constant C will have the same value in all layers.

An axial load N and an axial spring with stiffness K are applied at the reference point (RP). It should be noted that N is an applied load, and integration of all the axial stresses $\sigma_{zz,i}$ over the cross-section would generally give a result that is different from N. A static equilibrium equation in z-direction may be formulated at $z = L$ for the cylinder in Figure 3 b). The equilibrium equation is given by

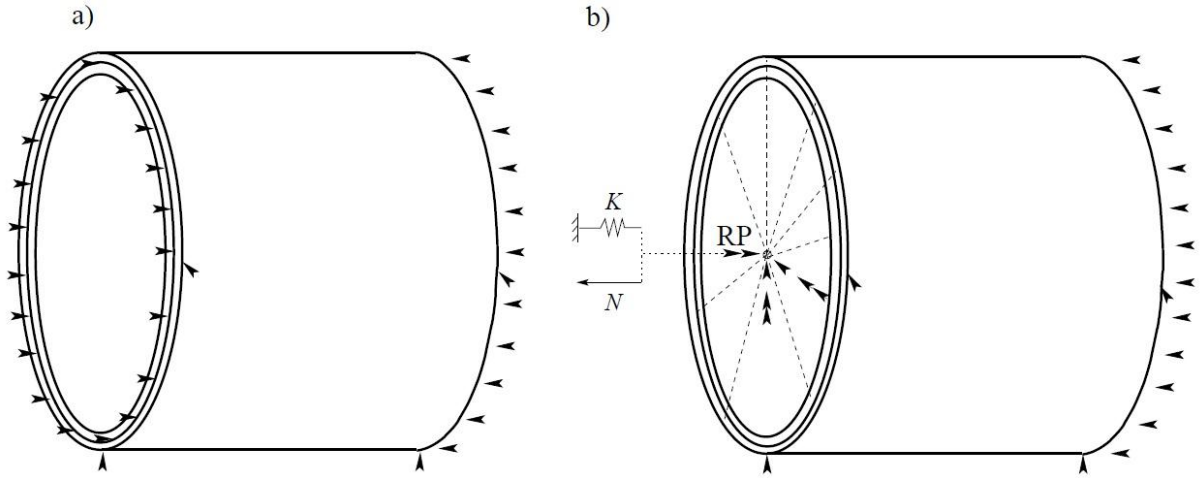

Figure 3 – Boundary conditions for: a) the axially fixed condition and b) the axially free condition with axial load *N* and axial spring *K*. Arrow heads indicate translational and double arrow heads rotational constraints.

$$\sum_{i=1}^{n}\left(\sigma_{zz,i}A_{s,i}\right) = -K \cdot u_z(L) + N, \tag{6}$$

where $A_{s,i} = \pi t_i(2r_i - t_i)$ is the cross-sectional area of the i-th layer, t_i is the thickness of the i-th layer and $u_z(L)$ is the axial displacement at $z = L$.

2.4 Boundary Conditions for Piping and Pipelines

In order to identify relevant boundary conditions for pipes and piping, it is useful to consider a typical piping or pipeline scenario, as illustrated by Figure 4. In Figure 4 c), a segment, or cut-out, of a piping system (Figure 4 a) or pipeline (Figure 4 b) is shown. Regardless of whether the cut-out is taken from a pipeline or a piping system, some axial stiffness is provided by axial interaction with the rest of the system. In addition, for subsea pipelines that are resting on the seabed, the axial friction is often modeled by springs with axial stiffness dependent on the soil type. Hence, spring stiffness is introduced in axial direction. However, in many cases the action on a pipe segment by its surroundings is represented by an applied load N rather than by axial springs. For example, at lay-down (i.e.,

just after installation) a subsea pipeline will have a residual lay tension and some non-zero axial strain, which implies that the pipe segment should be modeled with an external load N and no spring stiffness. When operational loads subsequently are applied, the degree of axial restraint may vary from zero (close to a spool or other flexible structure) to fully fixed (when the accumulated soil friction is large enough to fully restrain the pipe). For axial restraints in-between zero and full fixation, the pipe segment may be modeled with axial springs. The spring stiffness will depend on e.g., the stiffness properties of the soil and the length L of the considered pipe segment. Thus, in order to facilitate the different manners of modeling the pipe segment's interaction with its surroundings, the problem has been idealized as shown in Figure 4 c). In the figure, an axial section force P acts on both ends of the pipe segment and includes potential contributions from both a spring force and an applied axial load. The section force may be expressed by

$$P = -k \cdot u_z(z_e) + N, \tag{7}$$

where $u_z(z_e)$ denotes the axial displacement of either cylinder end.

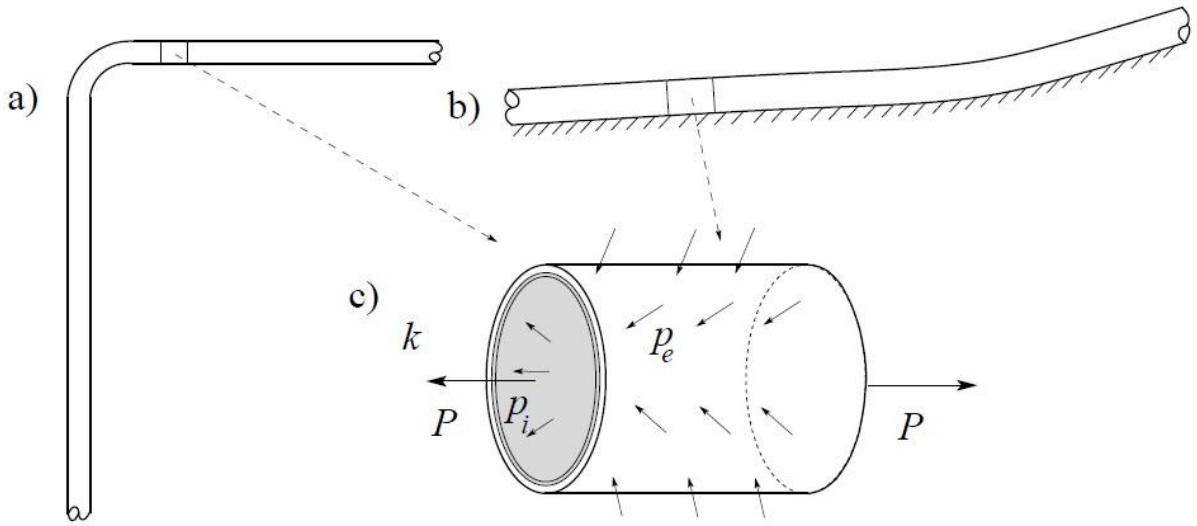

Figure 4 –a) Typical part of a two layer piping system configuration. b) Typical scenario for a two layer submarine pipeline resting on the seabed. c) Model of a pipe segment applicable to both scenario a) and scenario b).

From Eq. (7), one may observe that there is a spring with stiffness k mounted to each end of the pipe segment in Figure 4 c). It should be noted that the system in Figure 4 c) corresponds to the system in Figure 3 a) when $k \rightarrow \infty$. Moreover, the system in Figure 4 c) may be retrieved from the system in Figure 3 b) by setting $K = k/2$, or by setting $K = k$ while adjusting the length of the cylinder from L to $L/2$. The latter is evident from symmetry. Thus,

the boundary conditions for the pipe segment in Figure 4 c) are equivalent to the boundary conditions illustrated previously by Figure 3.

3 DISPLACEMENT ASSUMPTIONS

We aim to determine the exact three-dimensional stress state described in cylindrical coordinates as defined in Figure 1, for multi-layer cylinders subjected to pressure, thermal loading and axial loading, with boundary conditions as presented in the preceding section. In order to achieve this, the form of the displacement field must be known. For a cylinder exposed to internal and external pressure, an equilibrium equation in radial direction may be derived based on Figure 5, which displays the radial and hoop stresses acting on an infinitesimal element in a plane perpendicular to the cylinder axis (*z*-axis).

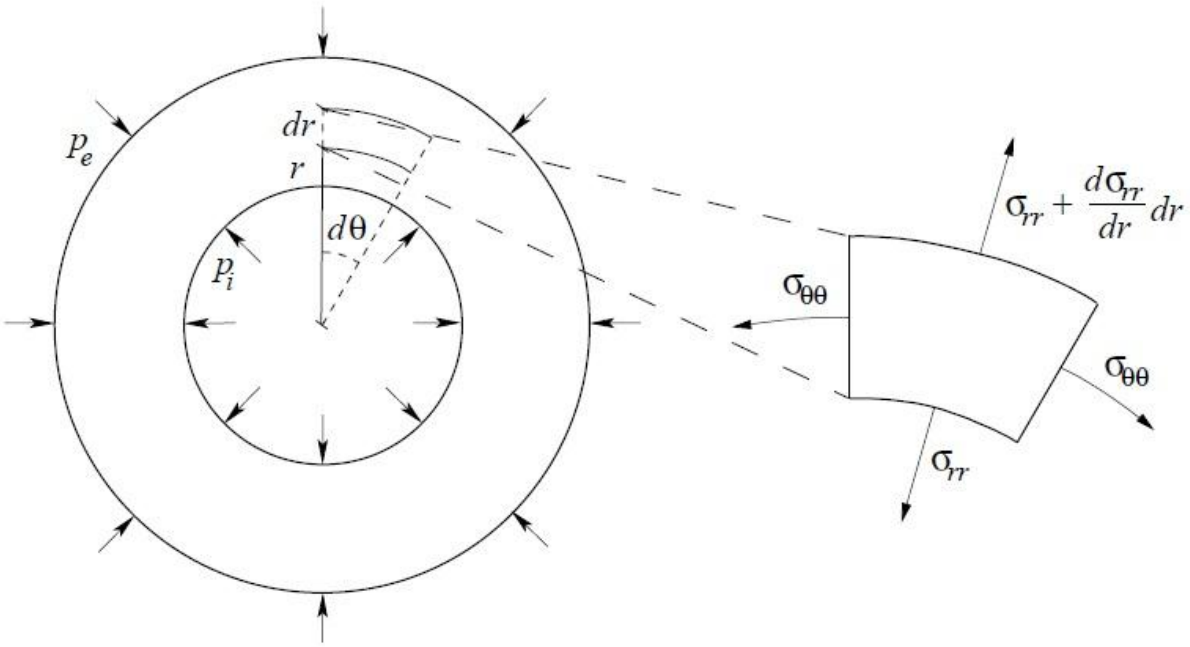

Figure 5 - A thick-walled ring subjected to internal and external pressure.

Since the internal and external pressures are uniformly distributed along the circumference, the resulting deformation will be symmetric about the axis of the cylinder, i.e.,

$$u_\theta = 0\,, \tag{8}$$

and the shear stresses $\tau_{r\theta}$ will be zero. Moreover, the shear stresses τ_{rz} will be zero since the thermal loading and pressures are uniform in axial direction and the axial displacements according to assumption (viii) and (ix) (Section 2.1) are constant, either in each individual layer (plane stress) or over the entire cross-section (plane strain and generalized plane strain).

Noting that $\sin(d\theta) \approx d\theta$ the following equilibrium equation can then be formulated in the radial direction for the element displayed in Figure 5:

$$\sigma_{rr} r d\theta + \sigma_{\theta\theta} dr d\theta - \left(\sigma_{rr} + \frac{d\sigma_{rr}}{dr} dr \right)(r + dr) d\theta = 0 \quad \textbf{(9)}$$

By ignoring higher-order quantities one obtains

$$\sigma_{\theta\theta} - \sigma_{rr} - r \frac{d\sigma_{rr}}{dr} = 0 \quad \textbf{(10)}$$

The equilibrium equation in radial direction, Eq. (10), may subsequently be applied to derive the differential equation for the radial displacement u_r for plane stress (*i*) and plane strain (*ii*) conditions. The case of plane stress will be examined first. Hooke's material law for plane stress is given by

$$\begin{bmatrix} \sigma_{rr} \\ \sigma_{\theta\theta} \end{bmatrix} = \frac{E}{1-\nu^2} \begin{bmatrix} 1 & \nu \\ \nu & 1 \end{bmatrix} \begin{bmatrix} \varepsilon_{rr} \\ \varepsilon_{\theta\theta} \end{bmatrix} \quad \textbf{(11)}$$

where E is the Young's modulus and ν the Poisson's ratio for the cylinder wall material.

The radial strain ε_{rr} and hoop strain $\varepsilon_{\theta\theta}$ in cylindrical coordinates are given by

$$\begin{aligned} \varepsilon_{rr} &= \frac{du_r}{dr} \\ \varepsilon_{\theta\theta} &= \frac{1}{r}\frac{\partial u_\theta}{\partial \theta} + \frac{1}{r} u_r = \frac{u_r}{r} \end{aligned} \quad \textbf{(12)}$$

where the simplified expression for the $\varepsilon_{\theta\theta}$ hoop strain follows from Eq. (8). By inserting the stress expressions from Eq. (11) into Eq. (10), the following differential equation for the radial displacement u_r is obtained:

$$\frac{d^2 u_r}{dr^2} + \frac{1}{r}\frac{du_r}{dr} - \frac{u_r}{r^2} = 0 \quad \textbf{(13)}$$

The general solution of the differential equation is

$$u_r = \frac{C_{r1}}{r} + C_{r2} r \quad \textbf{(14)}$$

which may be verified by substitution.

In the case of plane strain, the material law becomes

$$\begin{bmatrix} \sigma_{rr} \\ \sigma_{\theta\theta} \end{bmatrix} = \frac{E}{(1+\nu)(1-2\nu)} \begin{bmatrix} 1-\nu & \nu \\ \nu & 1-\nu \end{bmatrix} \begin{bmatrix} \varepsilon_{rr} \\ \varepsilon_{\theta\theta} \end{bmatrix} \quad \textbf{(15)}$$

The strains may be expressed in terms of the radial displacement by using Eq. (12), and inserted into the material law given by Eq. (15). By inserting the resulting stresses into the equilibrium equation, Eq. (10), the same differential equation, Eq. (13), as was found for plane stress is retrieved for the plane strain condition. Hence, the general solution given in Eq. (14) applies for both plane stress and plane strain. The two displacement field coefficients C_{r1}

and C_{r2} may now be obtained by inserting the expression for u_r in Eq. (14) into Eqs. (11) and (15), and applying the boundary conditions at the inner and outer cylinder surfaces, i.e., Eqs. (1) and (2).

From Eqs. (11), (14) and (15) it is also easily demonstrated that the sum of radial stress σ_{rr} and hoop stress $\sigma_{\theta\theta}$ is constant, i.e., independent of r. Since the Poisson expansion in the axial direction thus will be uniform over the cylinder cross-section, a two-dimensional treatment of the problem is justified. The displacement field given by Eq. (14) is commonly termed the Lamé displacement field, since the solution outlined above for radial and hoop stresses in a pressurized cylinder was first derived by Lamé and Clapeyron [1831].

In a multi-layer cylinder, each layer may have different material properties (e.g., Young's modulus E, Poisson's ratio ν and coefficient of thermal expansion α). Consequently, the response to thermal loading and pressure loading will be different in each layer, and contact pressures q_i will therefore be created between the layers (in the case that an inner cylinder expands less than the adjacent outer cylinder, q_i will be a tensile contact stress rather than a contact pressure, assuming that the layers are tightly bonded in the radial direction). For plane stress and plane strain conditions, each single layer may be modeled as a cylinder subjected to internal pressure q_{i-1} and external pressure q_i. This is just the same situation as described for the pressurized cylinder shown in Figure 5, and although the pressures q_i are undetermined at this stage, it is evident that the displacement field in each layer must have the same form as given by Eqs. (8) and (14), i.e.,

$$\begin{aligned} u_{r,j} &= \frac{C_{r1,i}}{r} + C_{r2,i} r \\ u_{\theta,j} &= 0 \end{aligned} \qquad \textbf{(16)}$$

The final axial boundary condition that needs to be examined is the case of a spring-mounted cylinder subjected to an axial load. It was described in the preceding section that the cylinder layers are assumed tightly fitted in the axial direction, i.e., no sliding occurs (which is opposite to the plane stress case, where the layers are assumed to slide freely relative to each other). Hence, the axial strain will be uniform over the entire multi-layer cross-section:

$$\varepsilon_{zz,i} = \frac{\partial u_{z,i}}{\partial z} = C \qquad \textbf{(17)}$$

where C is constant for all layers and thus independent of i. It should be noted that plane strain, which was discussed above, is the special case in which $C = 0$. Solving the differential equation above, Eq. (17), with respect to the spring-mounted boundary condition yields the displacement field of a bar:

$$u_{z,j} = u_z = C_z \frac{z}{L} \tag{18}$$

In Eq. (18), u_z is the displacement field in z-direction, L is the length of the cylinder segment and C_z is an undetermined coefficient.

Either plane stress or plane strain was assumed when deriving the Lamé displacement field, Eq. (14), for the radial displacement. In the case of generalized plane strain, each layer may be modeled as a cylinder that is subjected to internal pressure $q_{i\text{-}1}$, external pressure q_i and an axial load. The axial loading is uniform over each individual layer since heat and direct axial loading are applied uniformly. However, it has been shown by Vedeld and Sollund [2013] that the Lamé displacement field is still an exact representation of the radial displacement for a cylinder subjected to axisymmetric pressure loading and a uniform axial load, even when a fully three-dimensional material law applies. Consequently, the full displacement field for the *i*-th layer in the generalized plane strain case is given by Eqs. (16) and (18).

4 STRESS AND STRAIN RELATIONS

The displacement fields for relevant axial boundary conditions were determined in the previous section. The full displacement field applicable for all the boundary conditions may be written as

$$\begin{aligned} u_{r,i} &= \frac{C_{r1,i}}{r} + C_{r2,i} r \\ u_{\theta,i} &= 0 \\ u_{z,i} &= C_{z,i} \frac{z}{L} \end{aligned} \tag{19}$$

where $C_{z,i} = 0$ for plane strain and $C_{z,i} = C_z$ is the same for all layers for the spring-mounted cylinder. For the plane stress case $C_{z,i}$ will generally not be solved for, since the axial stress state ($\sigma_{zz,i} = 0$) is already known in each layer.

The strain field in cylindrical coordinates is given by [Cook et al., 2002]

$$\begin{aligned} \varepsilon_{rr,i} &= \frac{\partial u_{r,i}}{\partial r} = -\frac{C_{r1,i}}{r^2} + C_{r2,i} \\ \varepsilon_{\theta\theta,i} &= \frac{1}{r}\frac{\partial u_{\theta,i}}{\partial \theta} + \frac{1}{r} u_{r,i} = \frac{C_{r1,i}}{r^2} + C_{r2,i} \\ \varepsilon_{zz,i} &= \frac{\partial u_{z,i}}{\partial z} = \frac{C_{z,i}}{L} \\ \gamma_{r\theta,i} &= \frac{1}{r}\frac{\partial u_{r,i}}{\partial \theta} + \frac{\partial u_{\theta,i}}{\partial r} - \frac{u_{\theta,i}}{r} = 0 \\ \gamma_{\theta z,i} &= \frac{\partial u_{\theta,i}}{\partial z} + \frac{1}{r}\frac{\partial u_{z,i}}{\partial \theta} = 0 \\ \gamma_{rz,i} &= \frac{\partial u_{r,i}}{\partial z} + \frac{\partial u_{z,i}}{\partial r} = 0 \end{aligned} \tag{20}$$

In Eq. (20), $\varepsilon_{ij,i}$ are normal strains and $\gamma_{ij,i}$ are shear strains in the i-th layer of the multi-layer cylinder. It is noted from Eq. (20) that all the shear strain terms vanish. Consequently, the strain tensor may be represented by

$$\boldsymbol{\varepsilon}_i = \begin{bmatrix} \varepsilon_{rr,i} \\ \varepsilon_{\theta\theta,i} \\ \varepsilon_{zz,i} \end{bmatrix} = \begin{bmatrix} \dfrac{\partial u_{r,i}}{\partial r} \\ \dfrac{u_{r,i}}{r} \\ \dfrac{\partial u_{z,i}}{\partial z} \end{bmatrix} \tag{21}$$

The temperature-induced stresses can either be accounted for as initial stresses or indirectly as initial strains. In the present study, it is chosen to apply the thermal loadings as initial strains. Consequently, the associated stresses become:

$$\boldsymbol{\sigma}_i = \mathbf{E}_i\left(\boldsymbol{\varepsilon}_i - \boldsymbol{\varepsilon}_{0,i}\right) + \boldsymbol{\sigma}_{0,i} \tag{22}$$

where $\boldsymbol{\sigma}_{0,i} = \mathbf{0}$. The initial strains in the i-th cylinder layer are found by simple temperature expansion:

$$\varepsilon_{rr,i}^0 = \varepsilon_{\theta\theta,i}^0 = \varepsilon_{zz,i}^0 = \alpha_i \Delta T_i \tag{23}$$

In Eq. (23), α_i is the temperature expansion coefficient and ΔT_i the temperature change of the i-th layer, and the superscripts "0" are included in order to indicate that they are initial strains. The generalized Young's modulus in Eq. (22) is given by

$$\mathbf{E}_i = \hat{E}_i \begin{bmatrix} 1-\nu_i & \nu_i & \nu_i \\ \nu_i & 1-\nu_i & \nu_i \\ \nu_i & \nu_i & 1-\nu_i \end{bmatrix}, \quad \text{where} \quad \hat{E}_i = \frac{E_i}{(1-2\nu_i)(1+\nu_i)} \tag{24}$$

In the absence of shear strains, the full three-dimensional stress state in the i-th layer of the multi-layer cylinder is thus given by

$$\begin{bmatrix} \sigma_{rr,i} \\ \sigma_{\theta\theta,i} \\ \sigma_{zz,i} \end{bmatrix} = \hat{E}_i \begin{bmatrix} 1-\nu_i & \nu_i & \nu_i \\ \nu_i & 1-\nu_i & \nu_i \\ \nu_i & \nu_i & 1-\nu_i \end{bmatrix} \begin{bmatrix} \dfrac{\partial u_{r,i}}{\partial r} - \alpha_i \Delta T_i \\ \dfrac{u_{r,i}}{r} - \alpha_i \Delta T_i \\ \dfrac{\partial u_{z,i}}{\partial z} - \alpha_i \Delta T_i \end{bmatrix}, \tag{25}$$

where $\sigma_{rr,i}$ is the radial stress, $\sigma_{\theta\theta,i}$ is the hoop stress, and $\sigma_{zz,i}$ is the axial stress of the i-th layer in the cylinder. After inserting for the displacement field, Eq. (19), into Eq. (25) the stress field becomes

$$\begin{bmatrix} \sigma_{rr,i} \\ \sigma_{\theta\theta,i} \\ \sigma_{zz,i} \end{bmatrix} = \hat{E}_i \begin{bmatrix} -(1-2\nu_i)\dfrac{C_{r1,i}}{r^2} + C_{r2,i} + \nu_i \dfrac{C_{z,i}}{L} - \alpha_i \Delta T_i (1+\nu_i) \\ (1-2\nu_i)\dfrac{C_{r1,i}}{r^2} + C_{r2,i} + \nu_i \dfrac{C_{z,i}}{L} - \alpha_i \Delta T_i (1+\nu_i) \\ 2\nu_i C_{r2,i} + (1-\nu_i)\dfrac{C_{z,i}}{L} - \alpha_i \Delta T_i (1+\nu_i) \end{bmatrix} \tag{26}$$

As noted in conjunction with Eq. (19), this formulation covers all the relevant boundary conditions, with only the coefficient $C_{z,i}$ treated differently in each case.

Interestingly, one may observe from Eq. (26) that

$$\frac{\sigma_{rr,i} + \sigma_{\theta\theta,i}}{2} = C_{r2,i} + \nu_i \frac{C_{z,i}}{L} - \alpha_i \Delta T_i (1+\nu_i). \tag{27}$$

In other words, the sum of the radial and hoop stresses is generally independent of the radial coordinate r, as was noted previously for a single thick-walled cylinder, subjected only to

internal and external pressure. Similarly, it is observed that the sum of the radial and hoop strains is constant:

$$\frac{\varepsilon_{rr,i} + \varepsilon_{\theta\theta,i}}{2} = \frac{1}{2}\left(\frac{\partial u_{r,i}}{\partial r} + \frac{u_{r,i}}{r}\right) = C_{r2,i} \ . \tag{28}$$

It is also easily shown from Eq. (25), by setting $\sigma_{zz,i} = 0$, solving for $(\partial u_{z,i}/\partial z - \alpha_i \Delta T_i)$ in terms of the two remaining strain components and inserting the solution into the equations for radial stress $\sigma_{rr,i}$ and hoop stress $\sigma_{\theta\theta,i}$, that the reduced stress state formula

$$\begin{bmatrix} \sigma_{rr,i} \\ \sigma_{\theta\theta,i} \end{bmatrix} = \frac{E_i}{1-\nu_i^2}\begin{bmatrix} 1 & \nu_i \\ \nu_i & 1 \end{bmatrix}\begin{bmatrix} \dfrac{\partial u_{r,i}}{\partial r} - \alpha_i \Delta T_i \\ \dfrac{u_{r,i}}{r} - \alpha_i \Delta T_i \end{bmatrix} \tag{29}$$

applies for the plane stress case. Eq. (29) may be recognized as identical to Eq. (15). After inserting for the radial displacement field, one obtains

$$\begin{bmatrix} \sigma_{rr,i} \\ \sigma_{\theta\theta,i} \end{bmatrix} = \frac{E_i}{1-\nu_i^2}\begin{bmatrix} -(1-\nu_i)\dfrac{C_{r1,i}}{r^2} + (1+\nu_i)C_{r2,i} - \alpha_i \Delta T_i (1+\nu_i) \\ (1-\nu_i)\dfrac{C_{r1,i}}{r^2} + (1+\nu_i)C_{r2,i} - \alpha_i \Delta T_i (1+\nu_i) \end{bmatrix} \tag{30}$$

From Eq. (30) it is clear that the stress state in the *i*-th layer of the cylinder, as expected, is independent of the axial displacement coefficient $C_{z,i}$.

5 ANALYTICAL SOLUTIONS BASED ON MATRIX INVERSION

5.1 Plane Stress

Analytical solutions for *n*-layer cylinders under pressure, temperature and axial loading are derived in the following. The solutions are not closed analytical solutions, but instead require matrix inversion. The plane stress condition is investigated first. Plane stress is relevant when the layers are axially free and there is negligible friction between the layers. Since each layer in this case is free to expand axially, the displacement field for each cylinder layer has three undetermined coefficients, as shown in Eq. (19). However, the axial coefficients $C_{z,j}$ are not required for a complete description of the stress state, as noted in the preceding section. In order to determine the radial and hoop stresses, we must therefore establish 2*n* equations.

The radial stresses at the innermost and outermost surfaces must be equal, with opposite sign, to the applied internal and external pressures, respectively:

$$\begin{aligned} &\sigma_{rr,1}(r_0) = -q_0 = -p_{int} \ , \\ &\sigma_{rr,n}(r_n) = -q_n = -p_{ext} \ . \end{aligned} \tag{31}$$

In Eq. (31), r_0 is the innermost radius of the multi-layer cross-section and r_n is the outer radius of the multi-layer cross-section, as shown in Figure 2. Similarly, q_0 is the known internal pressure (the pressure acting on the surface with radius r_0) and q_n the known external pressure (the pressure acting on the surface with radius r_n). From Eq. (30), the two relations in Eq. (31) may be expressed as displacement field coefficient equations by

$$\begin{aligned} &-\frac{E_1}{(1+\nu_1)r_0^2} C_{r1,1} + \frac{E_1}{1-\nu_1} C_{r2,1} = -q_0 + \frac{E_1}{1-\nu_1}\alpha_1 \Delta T_1 \ , \\ &-\frac{E_n}{(1+\nu_n)r_n^2} C_{r1,n} + \frac{E_n}{1-\nu_n} C_{r2,n} = -q_n + \frac{E_n}{1-\nu_n}\alpha_n \Delta T_n \ . \end{aligned} \tag{32}$$

The displacement field in radial direction must be continuous over the contact surfaces between two adjacent layers. This gives rise to *n*-1 equations:

$$u_{r,i}(r_i) = u_{r,i+1}(r_i), \quad i \in \{1,2,...,n-1\} \tag{33}$$

By inserting for Eq. (19) into Eq. (33), the general field coefficient equation can be formulated as

$$\frac{C_{r1,i}}{r_i} + C_{r2,i} r_i - \frac{C_{r1,i+1}}{r_i} - C_{r2,i+1} r_i = 0 \ , \quad i \in \{1,2,...,n-1\} \tag{34}$$

The radial stresses must equal the contact pressures at the layer interfaces, which in turn results in a continuous radial stress field across inter-layer boundaries. This gives rise to another n - 1 equations:

$$\sigma_{rr,i}(r_i) = \sigma_{rr,i+1}(r_i), \quad i \in \{1,2,...,n-1\} \tag{35}$$

From Eq. (30) it follows that Eq. (35) may be rewritten as the following field coefficient equation:

$$\begin{aligned} &-\frac{E_i}{1+\nu_i}\frac{C_{r1,i}}{r_i^2} + \frac{E_i}{1-\nu_i}C_{r2,i} + \frac{E_{i+1}}{1+\nu_{i+1}}\frac{C_{r1,i+1}}{r_i^2} - \frac{E_{i+1}}{1-\nu_{i+1}}C_{r2,i+1} \\ &= \frac{E_i}{1-\nu_i}\alpha_i \Delta T_i (1+\nu_i) - \frac{E_{i+1}}{1-\nu_{i+1}}\alpha_{i+1}\Delta T_{i+1}(1+\nu_{i+1}), \quad i \in \{1,2,...,n-1\} \end{aligned} \tag{36}$$

Eqs. (32), (34) and (36) form a system of 2n equations, which are sufficient to solve for the 2n displacement field coefficients. The system of equations may be written on matrix form as

$$\mathbf{KD} = \mathbf{R}, \tag{37}$$

where a stiffness matrix **K** has been defined by

$$\mathbf{K} = \begin{bmatrix} \mathbf{k}_0 & \mathbf{0} & \mathbf{0} & \cdots & \mathbf{0} & \mathbf{0} & \mathbf{0} & \mathbf{0} \\ \mathbf{k}_1^1 & \mathbf{k}_1^2 & \mathbf{0} & \cdots & \mathbf{0} & \mathbf{0} & \mathbf{0} & \mathbf{0} \\ \mathbf{0} & \mathbf{k}_2^1 & \mathbf{k}_2^2 & \cdots & \mathbf{0} & \mathbf{0} & \mathbf{0} & \mathbf{0} \\ \vdots & \vdots & \vdots & \ddots & \vdots & \vdots & \vdots & \vdots \\ \mathbf{0} & \mathbf{0} & \mathbf{0} & \cdots & \mathbf{k}_{n-3}^1 & \mathbf{k}_{n-3}^2 & \mathbf{0} & \mathbf{0} \\ \mathbf{0} & \mathbf{0} & \mathbf{0} & \cdots & \mathbf{0} & \mathbf{k}_{n-2}^1 & \mathbf{k}_{n-2}^2 & \mathbf{0} \\ \mathbf{0} & \mathbf{0} & \mathbf{0} & \cdots & \mathbf{0} & \mathbf{0} & \mathbf{k}_{n-1}^1 & \mathbf{k}_{n-1}^2 \\ \mathbf{0} & \mathbf{0} & \mathbf{0} & \cdots & \mathbf{0} & \mathbf{0} & \mathbf{0} & \mathbf{k}_n \end{bmatrix},$$

$$\mathbf{k}_0 = \begin{bmatrix} -\frac{E_1}{(1+\nu_1)r_0^2} & \frac{E_1}{1-\nu_1} \end{bmatrix}, \quad \mathbf{k}_i^1 = \begin{bmatrix} \frac{1}{r_i} & r_i \\ -\frac{E_i}{(1+\nu_i)r_i^2} & \frac{E_i}{1-\nu_i} \end{bmatrix}, \tag{38}$$

$$\mathbf{k}_i^2 = \begin{bmatrix} -\frac{1}{r_i} & -r_i \\ \frac{E_{i+1}}{(1+\nu_{i+1})r_i^2} & -\frac{E_{i+1}}{1-\nu_{i+1}} \end{bmatrix}, \quad \mathbf{k}_n = \begin{bmatrix} -\frac{E_n}{(1+\nu_n)r_n^2} & \frac{E_n}{1-\nu_n} \end{bmatrix},$$

while the displacement coefficient **D** is given by

$$\mathbf{D}^T = \begin{bmatrix} C_{r1,1} & C_{r2,1} & C_{r1,2} & C_{r2,2} & C_{r1,3} & \cdots & C_{r1,n} & C_{r2,n} \end{bmatrix}, \tag{39}$$

and the load vector **R** is given by

$$\mathbf{R}^T = \Bigg[-q_0 + \frac{E_1}{(1-\nu_1)}\alpha_1\Delta T_1 \quad 0 \quad \frac{E_1}{(1-\nu_1)}\alpha_1\Delta T_1 - \frac{E_2}{(1-\nu_2)}\alpha_2\Delta T_2 \quad \cdots$$
$$\cdots \quad 0 \quad \frac{E_{n-1}}{(1-\nu_{n-1})}\alpha_{n-1}\Delta T_{n-1} - \frac{E_n}{(1-\nu_n)}\alpha_n\Delta T_n \quad -q_n + \frac{E_n}{(1-\nu_n)}\alpha_n\Delta T_n \Bigg]. \tag{40}$$

Generally, the matrix equation, Eq. (37), is a pentadiagonal system and for $k = 2i$, the k-th row in the matrix is given by Eq. (34). Similarly, for $k = 2i+1$, the k-th row in the matrix is given by Eq. (36).

5.2 Plane Strain

A multi-layer cylinder that is fully restrained axially will be in a condition of plane strain. As in the case of plane stress, all the unknown displacement field coefficients may be determined by solving Eqs. (31), (33) and (35), which together comprise a system of $2n$ equations. However, since the plane stress material law, Eq. (30), is no longer applicable, the system of equations will be different. The stress state in layer i is now given by Eq. (26), with $C_{z,i} = 0$.

The boundary conditions on the inner and outer cylinder surfaces, Eq. (31), give the following relations:

$$\begin{aligned} -\frac{1-2\nu_1}{r_0^2}\hat{E}_1 C_{r1,1} + \hat{E}_1 C_{r2,1} &= -q_0 + \hat{E}_1\alpha_1\Delta T_1(1+\nu_1) \\ -\frac{1-2\nu_n}{r_n^2}\hat{E}_n C_{r1,n} + \hat{E}_n C_{r2,n} &= -q_n + \hat{E}_n\alpha_n\Delta T_n(1+\nu_n) \end{aligned} \tag{41}$$

Since the form of the radial displacement field u_r is the same as in the case of plane stress, the equation for continuous radial displacement across the layer boundaries, Eq. (34), is unchanged. The equation for continuous radial stresses across layer boundaries, Eq. (36), does change, and may now be written as

$$\begin{aligned} &-\frac{1-2\nu_i}{r_i^2}\hat{E}_i C_{r1,i} + \hat{E}_i C_{r2,i} + \frac{1-2\nu_{i+1}}{r_i^2}\hat{E}_{i+1} C_{r1,i+1} - \hat{E}_{i+1} C_{r2,i+1} \\ &= \hat{E}_i\alpha_i\Delta T_i(1+\nu_i) - \hat{E}_{i+1}\alpha_{i+1}\Delta T_{i+1}(1+\nu_{i+1}), \quad i \in \{1,2,\ldots,n-1\} \end{aligned} \tag{42}$$

As mentioned above, a system of $2n$ equations can be established from Eqs. (34), (41) and (42). The system of equations is written on matrix form below:

$$\mathbf{KD} = \mathbf{R}, \tag{43}$$

where a stiffness matrix **K** has been defined by

$$\mathbf{K}=\begin{bmatrix}
\mathbf{k}_0 & \mathbf{0} & \mathbf{0} & \cdots & \mathbf{0} & \mathbf{0} & \mathbf{0} & \mathbf{0} \\
\mathbf{k}_1^1 & \mathbf{k}_1^2 & \mathbf{0} & \cdots & \mathbf{0} & \mathbf{0} & \mathbf{0} & \mathbf{0} \\
\mathbf{0} & \mathbf{k}_2^1 & \mathbf{k}_2^2 & \cdots & \mathbf{0} & \mathbf{0} & \mathbf{0} & \mathbf{0} \\
\vdots & \vdots & \vdots & \ddots & \vdots & \vdots & \vdots & \vdots \\
\mathbf{0} & \mathbf{0} & \mathbf{0} & \cdots & \mathbf{k}_{n-3}^1 & \mathbf{k}_{n-3}^2 & \mathbf{0} & \mathbf{0} \\
\mathbf{0} & \mathbf{0} & \mathbf{0} & \cdots & \mathbf{0} & \mathbf{k}_{n-2}^1 & \mathbf{k}_{n-2}^2 & \mathbf{0} \\
\mathbf{0} & \mathbf{0} & \mathbf{0} & \cdots & \mathbf{0} & \mathbf{0} & \mathbf{k}_{n-1}^1 & \mathbf{k}_{n-1}^2 \\
\mathbf{0} & \mathbf{0} & \mathbf{0} & \cdots & \mathbf{0} & \mathbf{0} & \mathbf{0} & \mathbf{k}_n
\end{bmatrix},$$

$$\mathbf{k}_0=\begin{bmatrix} -\dfrac{1-2\nu_1}{r_0^2}\hat{E}_1 & \hat{E}_1 \end{bmatrix},\quad \mathbf{k}_i^1=\begin{bmatrix} \dfrac{1}{r_i} & r_i \\ -\dfrac{1-2\nu_i}{r_i^2}\hat{E}_i & \hat{E}_i \end{bmatrix},$$

$$\mathbf{k}_i^2=\begin{bmatrix} -\dfrac{1}{r_i} & -r_i \\ \dfrac{1-2\nu_{i+1}}{r_i^2}\hat{E}_{i+1} & -\hat{E}_{i+1} \end{bmatrix},\quad \mathbf{k}_n=\begin{bmatrix} -\dfrac{1-2\nu_n}{r_n^2}\hat{E}_n & \hat{E}_n \end{bmatrix}, \tag{44}$$

while the displacement coefficient **D** is given by

$$\mathbf{D}^T=\begin{bmatrix} C_{r1,1} & C_{r2,1} & C_{r1,2} & C_{r2,2} & C_{r1,3} & \cdots & C_{r1,n} & C_{r2,n} \end{bmatrix}, \tag{45}$$

and the load vector **R** is given by

$$\begin{aligned}\mathbf{R}^T=\Big[&-q_0+\hat{E}_1\alpha_1\Delta T_1(1+\nu_1) \quad 0 \quad \hat{E}_1\alpha_1\Delta T_1(1+\nu_1)-\hat{E}_2\alpha_2\Delta T_2(1+\nu_2) \quad \cdots \\ \cdots \quad &0 \quad \hat{E}_{n-1}\alpha_{n-1}\Delta T_{n-1}(1+\nu_{n-1})-\hat{E}_n\alpha_n\Delta T_n(1+\nu_n) \quad -q_n+\hat{E}_n\alpha_n\Delta T_n(1+\nu_n)\Big]\end{aligned} \tag{46}$$

As in the plane stress case, the matrix equation, Eq. (43), is a pentadiagonal system and for $k = 2i$, the k-th row in the matrix is given by Eq. (34). Similarly, for $k = 2i+1$, the k-th row in the matrix is given by Eq. (42).

5.3 Generalized Plane Strain with Axial Loading and Axial Spring

The case of generalized plane strain, where the multi-layer cylinder is spring-mounted and subjected to axial loading, is examined last. The layers are assumed tightly bonded (i.e., no relative sliding), and $C_{z,i} = C_z$ is therefore constant for all the layers. Since C_z in this case must be solved for, the number of required equations will be $2n + 1$. Eqs. (31), (33) and (35) still apply, and the material law in Eq. (26) should be used for the i-th layer. Eq. (31) may then be written as

$$
\begin{aligned}
&-\frac{1-2\nu_1}{r_0^2}\hat{E}_1 C_{r1,1} + \hat{E}_1 C_{r2,1} + \frac{\hat{E}_1\nu_1}{L} C_z = -q_0 + \hat{E}_1\alpha_1\Delta T_1(1+\nu_1),\\
&-\frac{1-2\nu_n}{r_n^2}\hat{E}_n C_{r1,n} + \hat{E}_n C_{r2,n} + \frac{\hat{E}_n\nu_n}{L} C_z = -q_n + \hat{E}_n\alpha_n\Delta T_n(1+\nu_n).
\end{aligned}
\tag{47}
$$

Eq. (34) is again valid for ensuring a continuous displacement function in radial direction. Continuous radial stresses across layer boundaries may be ensured by requiring that

$$
\begin{aligned}
&-\frac{\hat{E}_i(1-2\nu_i)}{r_i^2} C_{r1,i} + \hat{E}_i C_{r2,i} + \frac{C_{r1,i+1}(1-2\nu_{i+1})}{r_i^2}\hat{E}_{i+1} - \hat{E}_{i+1} C_{r2,i+1} + \frac{\hat{E}_i\nu_i - \hat{E}_{i+1}\nu_{i+1}}{L} C_z\\
&= \hat{E}_i\alpha_i\Delta T_i(1+\nu_i) - \hat{E}_{i+1}\alpha_{i+1}\Delta T_{i+1}(1+\nu_{i+1}), \quad i \in \{1,2,...,n-1\}
\end{aligned}
\tag{48}
$$

Eqs. (34), (47) and (48) together give a system of $2n$ equations. Thus, one more equation is needed, which may be obtained from equilibrium in axial direction at the spring-mounted end:

$$
\sum_{i=1}^{n}\sigma_{zz,i}A_{s,i} = -Ku_z(L) + N = -KC_z + N\,. \tag{49}
$$

In Eq. (49), $A_{s,i}$ is the cross-sectional area of a single layer defined by $A_{s,i} = \pi t_i(2r_{i+1} - t_i)$, where $t_i = r_{i+1} - r_i$. The resulting field coefficient equation is

$$
2\sum_{i=1}^{n}\nu_i\hat{E}_i A_{s,i} C_{r2,i} + K_z C_z = R_z\,, \tag{50}
$$

where

$$
K_z = K + \frac{\sum_{i=1}^{n}(1-\nu_i)\hat{E}_i A_{s,i}}{L} \quad \text{and} \quad R_z = N + \sum_{i=1}^{n}\alpha_i\Delta T_i(1+\nu_i)\hat{E}_i A_{s,i} \tag{51}
$$

The total system of $(2n + 1)$ equations may be written on matrix form as

$$
\mathbf{KD} = \mathbf{R}\,, \tag{52}
$$

where a stiffness matrix **K** in this case has been defined by

$$\mathbf{K}=\begin{bmatrix}
\mathbf{k}_0 & \mathbf{0} & \mathbf{0} & \cdots & \mathbf{0} & \mathbf{0} & \mathbf{0} & \mathbf{0} & \dfrac{\hat{E}_1\nu_1}{L} \\
\mathbf{k}_1^1 & \mathbf{k}_1^2 & \mathbf{0} & \cdots & \mathbf{0} & \mathbf{0} & \mathbf{0} & \mathbf{0} & \mathbf{k}_1^3 \\
\mathbf{0} & \mathbf{k}_2^1 & \mathbf{k}_2^2 & \cdots & \mathbf{0} & \mathbf{0} & \mathbf{0} & \mathbf{0} & \mathbf{k}_2^3 \\
\vdots & \vdots & \vdots & \ddots & \vdots & \vdots & \vdots & \vdots & \vdots \\
\mathbf{0} & \mathbf{0} & \mathbf{0} & \cdots & \mathbf{k}_{n-3}^1 & \mathbf{k}_{n-3}^2 & \mathbf{0} & \mathbf{0} & \mathbf{k}_{n-3}^3 \\
\mathbf{0} & \mathbf{0} & \mathbf{0} & \cdots & \mathbf{0} & \mathbf{k}_{n-2}^1 & \mathbf{k}_{n-2}^2 & \mathbf{0} & \mathbf{k}_{n-2}^3 \\
\mathbf{0} & \mathbf{0} & \mathbf{0} & \cdots & \mathbf{0} & \mathbf{0} & \mathbf{k}_{n-1}^1 & \mathbf{k}_{n-1}^2 & \mathbf{k}_{n-1}^3 \\
\mathbf{0} & \mathbf{0} & \mathbf{0} & \cdots & \mathbf{0} & \mathbf{0} & \mathbf{0} & \mathbf{k}_n & \dfrac{\hat{E}_n\nu_n}{L} \\
\mathbf{k}_1^4 & \mathbf{k}_2^4 & \mathbf{k}_3^4 & \cdots & \mathbf{k}_{n-3}^4 & \mathbf{k}_{n-2}^4 & \mathbf{k}_{n-1}^4 & \mathbf{k}_n^4 & K_z
\end{bmatrix}, \tag{53}$$

$$\mathbf{k}_i^3=\begin{bmatrix}0\\ \dfrac{\hat{E}_i\nu_i-\hat{E}_{i+1}\nu_{i+1}}{L}\end{bmatrix},\quad \mathbf{k}_i^4=\begin{bmatrix}0 & 2\nu_i\hat{E}_iA_{s,i}\end{bmatrix},$$

and where $\mathbf{k}_0$, $\mathbf{k}_n$, $\mathbf{k}_i^1$ and $\mathbf{k}_i^2$ are taken from Eq. (44). The following expression for the displacement coefficient **D** applies:

$$\mathbf{D}^T=\begin{bmatrix}C_{r1,1} & C_{r2,1} & C_{r1,2} & C_{r2,2} & C_{r1,3} & \cdots & C_{r1,n} & C_{r1,n} & C_z\end{bmatrix}, \tag{54}$$

while the load vector **R** may be expressed by

$$\begin{aligned}\mathbf{R}^T=\Big[&-p_i+\hat{E}_1\alpha_1\Delta T_1(1+\nu_1) \quad 0 \quad \hat{E}_1\alpha_1\Delta T_1(1+\nu_1)-\hat{E}_2\alpha_2\Delta T_2(1+\nu_2) \quad \cdots \\ \cdots \quad &0 \quad \hat{E}_{n-1}\alpha_{n-1}\Delta T_{n-1}(1+\nu_{n-1})-\hat{E}_n\alpha_n\Delta T_n(1+\nu_n) \quad -p_e+\hat{E}_n\alpha_n\Delta T_n(1+\nu_n) \quad R_z\Big]\end{aligned} \tag{55}$$

6 ANALYTICAL SOLUTION BASED ON ITERATION

6.1 Plane Stress and Plane Strain

In order to derive an efficient iterative solution for the displacement field coefficients of a multi-layer cylinder, it is convenient to introduce some new notation. Thus, we start by defining the stresses, which in the new notation will be given by

$$\begin{bmatrix} \sigma_{rr,i} \\ \sigma_{\theta\theta,i} \\ \sigma_{zz,i} \end{bmatrix} = \begin{bmatrix} \dfrac{A_i}{r^2} + C_i - \varphi_i \\ -\dfrac{A_i}{r^2} + C_i - \varphi_i \\ \psi_i \end{bmatrix}, \tag{56}$$

where for plane stress

$$\begin{aligned} &A_i = \frac{-E_i}{1+\nu_i} C_{r1,i} \quad \text{and} \quad C_i = \frac{E_i}{1-\nu_i} C_{r2.i} \,, \\ &\varphi_i = \hat{E}_i \alpha_i \Delta T_i (1+\nu_i) \quad \text{and} \quad \psi_i = 0 \,, \end{aligned} \tag{57}$$

and for plane strain

$$\begin{aligned} &A_i = -\hat{E}_i (1-2\nu_i) C_{r1,i} \quad \text{and} \quad C_i = \hat{E}_i C_{r2.i} \,, \\ &\varphi_i = \hat{E}_i \alpha_i \Delta T_i (1+\nu_i) \quad \text{and} \quad \psi_i = 2\nu_i C_i - \varphi_i \,. \end{aligned} \tag{58}$$

The expressions for A_i and φ_i are the same for the two conditions, while C_i and ψ_i are different. It is easily demonstrated that Eqs. (56) and (57) are equivalent to the plane stress material law given previously by Eq. (30). Similarly, it is straight-forward to check that Eqs. (56) and (58) correspond to Eq. (26) with $C_{z,i} = 0$.

We know from Section 3 that the radial displacement field in case of plane stress and plane strain will be given by the Lamé displacement field, which may be rewritten as

$$u_{r,i} = \lambda_i \frac{A_i}{r} + \beta_i C_i r \tag{59}$$

where

$$\lambda_i = -\frac{1}{\hat{E}_i (1-2\nu_i)} = -\frac{1+\nu_i}{E_i} \quad \text{and} \quad \beta_i = \begin{cases} \dfrac{1-\nu_i}{E_i} & \text{for plane stress.} \\ \dfrac{1}{\hat{E}_i} & \text{for plane strain.} \end{cases} \tag{60}$$

By inserting the expressions for A_i, C_i, λ_i and β_i into Eq. (59), it is observed that Eq. (59) is equivalent to the expression for radial displacement given in Eq. (19). Moreover, it is

observed that the only unknowns in Eqs. (56) - (60) above are $C_{r1,i}$ and $C_{r2,i}$, which are required for calculation of the newly introduced coefficients A_i and C_i. Hence, if we can calculate A_i and C_i, the stress state and displacement field in the multi-layer cylinder will be completely determined.

Like in Section 5, we require that the radial stresses and radial displacements must be continuous through the layer boundaries, in other words that

$$\begin{aligned} &\sigma_{rr}(r) \in \mathbf{C}[r_0, r_n] \;\Rightarrow\; \sigma_{rr,i}(r_i) = \sigma_{rr,i+1}(r_i), \\ &u_r(r) \in \mathbf{C}[r_0, r_n] \;\Rightarrow\; u_{r,i}(r_i) = u_{r,i+1}(r_i). \end{aligned} \tag{61}$$

By inserting the expressions for radial stresses and radial displacements given above into Eq. (61), the equation may be written as

$$\begin{aligned} &\frac{A_i}{r_i^2} + C_i - \hat{E}_i \alpha_i \Delta T_i (1+\nu_i) = \frac{A_{i+1}}{r_i^2} + C_{i+1} - \hat{E}_{i+1} \alpha_{i+1} \Delta T_{i+1} (1+\nu_{i+1}), \\ &\lambda_i \frac{A_i}{r_i} + \beta_i C_i r_i = \lambda_{i+1} \frac{A_{i+1}}{r_i} + \beta_{i+1} C_{i+1} r_i \,. \end{aligned} \tag{62}$$

Solving the set of two equations for A_{i+1} and C_{i+1} gives

$$\begin{aligned} A_{i+1} &= A_i \left(\frac{\lambda_i - \beta_{i+1}}{\lambda_{i+1} - \beta_{i+1}} \right) + C_i r_i^2 \left(\frac{\beta_i - \beta_{i+1}}{\lambda_{i+1} - \beta_{i+1}} \right) - \frac{\beta_{i+1} r_i^2 (\varphi_{i+1} - \varphi_i)}{\lambda_{i+1} - \beta_{i+1}}, \\ C_{i+1} &= \frac{A_i}{r_i^2} \left(\frac{\lambda_{i+1} - \lambda_i}{\lambda_{i+1} - \beta_{i+1}} \right) + C_i \left(\frac{\lambda_{i+1} - \beta_i}{\lambda_{i+1} - \beta_{i+1}} \right) + (\varphi_{i+1} - \varphi_i) \left(\frac{\lambda_{i+1}}{\lambda_{i+1} - \beta_{i+1}} \right). \end{aligned} \tag{63}$$

Since the contact pressure must be balanced by the radial stresses in each layer at the layer interfaces, the following two relations may be deduced for the contact pressure q_i:

$$\begin{aligned} &\sigma_{rr,i}(r_{i-1}) = -q_{i-1} \quad \Rightarrow \quad \frac{A_i}{r_{i-1}^2} + C_i - \varphi_i = -q_{i-1}, \\ &\sigma_{rr,i+1}(r_{i+1}) = -q_{i+1} \quad \Rightarrow \quad \frac{A_{i+1}}{r_{i+1}^2} + C_{i+1} - \varphi_{i+1} = -q_{i+1}. \end{aligned} \tag{64}$$

As described in Section 2.3, q_i is defined as the contact pressure between layers i and $i + 1$, and the internal pressure p_{int} and external pressure p_{ext} are defined as q_0 and q_n, respectively.

The expressions for A_{i+1} and C_{i+1} from Eq. (63) may subsequently be inserted into Eq. (64), which gives two equations in the variables A_i and C_i. Solving the system of two equations results in the following expressions for A_i and C_i:

$$\begin{aligned} \frac{A_i}{r_i^2} &= \gamma_i \frac{T_i q_{i-1} - q_{i+1}(\lambda_{i+1} - \beta_{i+1}) - \varphi_i(\beta_{i+1}\gamma_{i+1} - \lambda_{i+1}) - T_i \varphi_i - \varphi_{i+1}\beta_{i+1}(1-\gamma_{i+1})}{S_i - T_i}, \\ C_i &= \frac{-S_i q_{i-1} + q_{i+1}(\lambda_{i+1} - \beta_{i+1}) + \varphi_i(\beta_{i+1}\gamma_{i+1} - \lambda_{i+1}) + S_i \varphi_i + \varphi_{i+1}\beta_{i+1}(1-\gamma_{i+1})}{S_i - T_i}, \end{aligned} \tag{65}$$

where we have introduced

$$\begin{aligned} S_i &= (\lambda_i - \beta_{i+1})\gamma_{i+1}\gamma_i + (\lambda_{i+1} - \lambda_i)\gamma_i \,, \\ T_i &= \lambda_{i+1} - \beta_i + (\beta_i - \beta_{i+1})\gamma_{i+1} \,, \\ \gamma_{i+1} &= \frac{r_i^2}{r_{i+1}^2} \,. \end{aligned} \tag{66}$$

Again, it is convenient to utilize that the compressive radial stress on the interface between layers must equal the contact pressure. One may observe that

$$\sigma_{rr,i}(r_i) = -q_i \quad \Rightarrow \quad \frac{A_i}{r_i^2} + C_i - \varphi_i = -q_i \,, \tag{67}$$

which is equivalent to the second relation in Eq. (64), but restated for index *i*. By inserting the expressions for A_i and C_i from Eq. (65) into Eq. (67), we obtain the following expression for q_{i+1}:

$$q_{i+1} = \frac{(S_i - \gamma_i T_i)q_{i-1} - (S_i - T_i)q_i + (1-\gamma_{i+1})(1-\gamma_i)(\varphi_i\beta_i - \varphi_{i+1}\beta_{i+1})}{(1-\gamma_i)(\lambda_{i+1} - \beta_{i+1})} \,. \tag{68}$$

The expressions for A_i and C_i may be greatly simplified by inserting the above expression for q_{i+1} into Eq. (65), which gives

$$\begin{aligned} \frac{A_i}{r_i^2} &= \frac{\gamma_i(q_i - q_{i-1})}{1-\gamma_i} \,, \\ C_i &= \frac{(\gamma_i q_{i-1} - q_i)}{(1-\gamma_i)} + \varphi_i \,. \end{aligned} \tag{69}$$

Eq. (68) is a second-order recurrence relation in q_i with boundary conditions at the start and end of the sequence, where we know the internal and external pressures q_0 and q_n on the free surfaces. The recurrence relation is non-linear since the coefficients are dependent on *i*. Since the boundary conditions are found at the start and end of the recurrence relation, it is not at the moment formulated as an initial value problem. The solution strategy, which is based on the solution proposed by Xiang et al. [2006], is, however, to express q_i in terms of the initial values q_0 and q_1. In order to obtain this, we define the recurrence relations a_i and b_i by

$$\begin{aligned} a_{i+1} &= \frac{(S_i - \gamma_i T_i)a_{i-1} - (S_i - T_i)a_i}{(1-\gamma_i)(\lambda_{i+1} - \beta_{i+1})} \,, \\ b_{i+1} &= \frac{(S_i - \gamma_i T_i)b_{i-1} - (S_i - T_i)b_i}{(1-\gamma_i)(\lambda_{i+1} - \beta_{i+1})} + \frac{(1-\gamma_{i+1})(1-\gamma_i)(\varphi_i\beta_i - \varphi_{i+1}\beta_{i+1})}{q_0(1-\gamma_i)(\lambda_{i+1} - \beta_{i+1})} \,, \end{aligned} \tag{70}$$

with initial values given by

$$a_0 = 0, \quad a_1 = 1, \quad b_0 = 1, \quad b_1 = 0 \,. \tag{71}$$

The contact pressure q_i may now be expressed as

$$q_i = a_i q_1 + b_i q_0 . \tag{72}$$

The validity of Eq. (72) will in the following be proven by induction. Note, however, that by setting φ_i to zero for all i, the solution is equal to the solution of Xiang et al. [2006], where thermal stresses were not included. Note also that the solution presented by Xiang et al. [2006] was not proven in their publication, so the proof presented in this study serves as a proof for both the solution presented herein, and the solution of Xiang et al. [2006].

Since the recurrence relation in Eq. (68) is second order, the expression must first be shown to be correct for the two initial values. However, it follows directly from the initial values of a_i and b_i, Eq. (71), that

$$\begin{aligned} q_0 &= a_0 q_1 + b_0 q_0 = q_0 , \\ q_1 &= a_1 q_1 + b_1 q_0 = q_1 . \end{aligned} \tag{73}$$

Hence, Eq. (72) is valid for $i = 0$ and $i = 1$. If we now assume that Eq. (72) is true for terms ($i - 1$) and i, it is sufficient to demonstrate that this leads to the validity of term ($i + 1$). By inserting Eq. (70) into Eq. (72) one obtains

$$\begin{aligned} q_{i+1} &= a_{i+1} q_1 + b_{i+1} q_0 \\ &= \frac{(S_i - \gamma_i T_i) a_{i-1} - (S_i - T_i) a_i}{(1-\gamma_i)(\lambda_{i+1} - \beta_{i+1})} q_1 \\ &\quad + \left(\frac{(S_i - \gamma_i T_i) b_{i-1} - (S_i - T_i) b_i}{(1-\gamma_i)(\lambda_{i+1} - \beta_{i+1})} + \frac{(1-\gamma_{i+1})(1-\gamma_i)(\varphi_i \beta_i - \varphi_{i+1} \beta_{i+1})}{q_0 (1-\gamma_i)(\lambda_{i+1} - \beta_{i+1})} \right) q_0 . \end{aligned} \tag{74}$$

Sorting the terms gives

$$\begin{aligned} q_{i+1} &= \frac{(S_i - \gamma_i T_i)}{(1-\gamma_i)(\lambda_{i+1} - \beta_{i+1})} (a_{i-1} q_1 + b_{i-1} q_0) - \frac{(S_i - T_i)}{(1-\gamma_i)(\lambda_{i+1} - \beta_{i+1})} (a_i q_1 + b_i q_0) \\ &\quad + \frac{(1-\gamma_{i+1})(1-\gamma_i)(\varphi_i \beta_i - \varphi_{i+1} \beta_{i+1})}{(1-\gamma_i)(\lambda_{i+1} - \beta_{i+1})} . \end{aligned} \tag{75}$$

Since we have assumed that Eq. (72) is true for term ($i - 1$) and i, Eq. (75) can be rewritten as

$$q_{i+1} = \frac{(S_i - \gamma_i T_i) q_{i-1}}{(1-\gamma_i)(\lambda_{i+1} - \beta_{i+1})} - \frac{(S_i - T_i) q_i}{(1-\gamma_i)(\lambda_{i+1} - \beta_{i+1})} + \frac{(1-\gamma_{i+1})(1-\gamma_i)(\varphi_i \beta_i - \varphi_{i+1} \beta_{i+1})}{(1-\gamma_i)(\lambda_{i+1} - \beta_{i+1})} . \tag{76}$$

However, the above expression for q_{i+1} is obviously true, since it is identical to Eq. (68). Consequently, the proposed solution in Eq. (72) is proven by induction.

Since q_n is equal to the known external pressure p_e, Eq. (72) can be solved for q_n.

$$q_n = a_n q_1 + b_n q_0 . \tag{77}$$

By solving Eq. (77) for q_1, the final unknown in Eq. (72) can be eliminated. After inserting the resulting expression for q_1 into Eq. (72), the following expression for the contact pressure q_i is obtained:

$$q_i = \frac{a_i}{a_n} q_n + \left(b_i - \frac{b_n}{a_n} a_i \right) q_0 = \frac{a_i}{a_n} p_{ext} + \left(b_i - \frac{b_n}{a_n} a_i \right) p_{int} . \qquad \textbf{(78)}$$

To compute the sequence of individual contact pressures $\{q_i\}$, it is now sufficient to first determine $\{a_i\}$ and $\{b_i\}$ recursively from Eq. (70) and insert the relevant values into Eq. (78). When the contact pressures are known, the coefficients A_i and C_i can be determined from Eq. (69). As noted above, the complete stress state and displacement field of the multi-layer cylinder can then be calculated using Eqs. (56) and (59).

6.2 Generalized Plane Strain with Axial Loading and Axial Spring

For the spring-mounted (generalized plane strain) boundary condition, the stresses in the *i*-th cylinder layer are given in new notation by

$$\begin{bmatrix} \sigma_{rr,i} \\ \sigma_{\theta\theta,i} \\ \sigma_{zz,i} \end{bmatrix} = \begin{bmatrix} \dfrac{A_i}{r^2} + C_i - \mu_i \\ -\dfrac{A_i}{r^2} + C_i - \mu_i \\ 2\nu_i C_i + \hat{E}_i (1 - \nu_i) \varepsilon_{zz} - \varphi_i \end{bmatrix}, \qquad \textbf{(79)}$$

where A_i, C_i and φ_i are the same as defined by Eq. (58), while

$$\varepsilon_{zz} = \frac{C_z}{L} \qquad \text{and} \qquad \mu_i = \varphi_i - \hat{E}_i \nu_i \varepsilon_{zz} . \qquad \textbf{(80)}$$

It is straight-forward to show that Eq. (79) is equivalent to Eq. (26) with $C_{z,i} = C_z$. The radial displacements u_r are given by Eqs. (59) and (60), where the value of β_i given for plane strain applies also for the present case. As seen from Eq. (19), the longitudinal displacement may be expressed as

$$u_z = C_z \frac{z}{L} = \varepsilon_{zz} z . \qquad \textbf{(81)}$$

With regard to a full description of the stress state and displacement field of the multi-layer cylinder, it is sufficient to determine A_i, C_i and ε_{zz} since all other quantities are known.

The only difference in the expressions for radial stresses and displacements of the spring-mounted cylinder relative to the plane strain case described in Section 6.1 is that the term φ_i in the expression for radial stress in Eq. (56) has been replaced by a term μ_i, as seen

from Eq. (79). From the similarity of the formulae, combined with the general validity of the assumptions that radial stresses and radial displacements must be continuous across layer boundaries, it is obvious that Eqs. (61) - (69) still hold as long as every occurrence of the quantity φ_i is replaced by μ_i. The same is true for the expressions for the two sequences $\{a_i\}$ and $\{b_i\}$, given by Eqs. (70) and (71). However, these latter relations, which were introduced to express q_i in terms of the initial values q_0 and q_1, will be discussed in the following and therefore included below for ease-of-reference. The recurrence relations are given by

$$\begin{aligned} a_{i+1} &= \frac{(S_i - \gamma_i T_i)a_{i-1} - (S_i - T_i)a_i}{(1-\gamma_i)(\lambda_{i+1} - \beta_{i+1})}, \\ b_{i+1} &= \frac{(S_i - \gamma_i T_i)b_{i-1} - (S_i - T_i)b_i}{(1-\gamma_i)(\lambda_{i+1} - \beta_{i+1})} + \frac{(1-\gamma_{i+1})(1-\gamma_i)(\mu_i\beta_i - \mu_{i+1}\beta_{i+1})}{p_i(1-\gamma_i)(\lambda_{i+1} - \beta_{i+1})}, \end{aligned} \qquad \textbf{(82)}$$

with initial values

$$a_0 = 0, \quad a_1 = 1, \quad b_0 = 1, \quad b_1 = 0. \qquad \textbf{(83)}$$

The contact pressure q_i is then expressed as

$$q_i = a_i q_1 + b_i q_0 = \frac{a_i}{a_n} q_n + \left(b_i - \frac{b_n}{a_n} a_i \right) q_0. \qquad \textbf{(84)}$$

The validity of the recurrence relations for $\{a_i\}$ and $\{b_i\}$ in case of plane strain, Eq. (72), was proven by induction in Section 7.1. The proof obviously holds also for Eq. (84) above, since all the relevant expressions become identical by substituting μ_i with φ_i. However, calculation of $\{a_i\}$ and $\{b_i\}$ for plane stress and plain strain conditions was straight-forward, since all the relevant quantities were known. This is not the case for the spring-mounted cylinder, since each individual term b_i depends on the unknown variable ε_{zz}, as seen from the definition of μ_i, Eq. (80). In order to solve for ε_{zz}, $\{b_i\}$ is separated into two sub-sequences by

$$b_i = c_i + d_i \cdot \varepsilon_{zz}. \qquad \textbf{(85)}$$

Recurrence relations for the sequences $\{c_i\}$ and $\{d_i\}$ can easily be established by inspection of Eqs. (80) and (82). By first noting that

$$\mu_i\beta_i = \varphi_i\beta_i - \nu_i\varepsilon_{zz}, \qquad \textbf{(86)}$$

the recurrence relations are found to be

$$\begin{aligned} c_{i+1} &= \frac{(S_i - \gamma_i T_i)c_{i-1} - (S_i - T_i)c_i}{(1-\gamma_i)(\lambda_{i+1} - \beta_{i+1})} + \frac{(1-\gamma_{i+1})(\varphi_i\beta_i - \varphi_{i+1}\beta_{i+1})}{q_0(\lambda_{i+1} - \beta_{i+1})}, \\ d_{i+1} &= \frac{(S_i - \gamma_i T_i)d_{i-1} - (S_i - T_i)d_i}{(1-\gamma_i)(\lambda_{i+1} - \beta_{i+1})} - \frac{(1-\gamma_{i+1})(\nu_i - \nu_{i+1})}{q_0(\lambda_{i+1} - \beta_{i+1})}, \end{aligned} \qquad \textbf{(87)}$$

with initial values

$$c_0 = 1, \quad c_1 = 0, \quad d_0 = d_1 = 0. \tag{88}$$

It is observed that $\{c_i\}$ is exactly equal to the sequence $\{b_i\}$ from Eq. (70).

By inserting Eq. (85) into Eq. (84) we obtain

$$q_i = \frac{a_i}{a_n} q_n + \left(c_i - \frac{c_n}{a_n} a_i \right) q_0 + \left(d_i - \frac{d_n}{a_n} a_i \right) q_0 \varepsilon_{zz} . \tag{89}$$

Since the quantities λ_i, β_i, φ_i and γ_i are defined equivalently for the spring-mounted cylinder and for the cylinder with plane strain, the derived quantities S_i and T_i will also be the same in the two cases. Consequently, the sequences $\{a_i\}$ and $\{c_i\}$ defined by Eqs. (82) and (87) are identical to the sequences $\{a_i\}$ and $\{b_i\}$ defined by Eq. (70) for the case of plane strain. Moreover, this implies that the first two terms in Eq. (89) are equal to the expression for the contact pressure in the case of plane strain, given by Eq. (78). The plane strain contact pressure at interface i, termed q_i in Eq. (78), will in the following be termed q_i^0 and the contact pressure at interface i for the spring-mounted cylinder may then be expressed as

$$q_i = q_i^0 + \zeta_i \varepsilon_{zz} , \tag{90}$$

where

$$\zeta_i = \left(d_i - \frac{d_n}{a_n} a_i \right) q_0 . \tag{91}$$

Now that the contact pressure q_i is expressed in terms of ε_{zz}, we may express also A_i and C_i in terms of ε_{zz} by using Eq. (69) with φ_i replaced by μ_i. Hence, the only unknown in the expressions for the stress state of the cylinder is ε_{zz}, and ε_{zz} may be determined from an equilibrium equation. We have not yet considered equilibrium in the axial direction. The applied axial force must be in equilibrium at the spring-supported end, which implies that

$$\sum_{i=1}^{n} \sigma_{zz,i} \pi \left(r_i^2 - r_{i-1}^2 \right) = N - KL\varepsilon_{zz} . \tag{92}$$

From Eq. (79) the axial stresses are given by

$$
\begin{aligned}
\sigma_{zz,i} &= 2\nu_i C_i + \hat{E}_i(1-\nu_i)\varepsilon_{zz} - \varphi_i \\
&= 2\nu_i \frac{1}{1-\gamma_i}\left(\gamma_i q_{i-1} - q_i\right) + 2\nu_i \mu_i + \hat{E}_i(1-\nu_i)\varepsilon_{zz} - \varphi_i \\
&= 2\nu_i \frac{1}{1-\gamma_i}\left[\left(\gamma_i q_{i-1}^0 - q_i^0\right) + \left(\gamma_i \zeta_{i-1}\varepsilon_{zz} - \zeta_i \varepsilon_{zz}\right)\right] \\
&\qquad + 2\nu_i\left(\varphi_i - \hat{E}_i \nu_i \varepsilon_{zz}\right) + \hat{E}_i(1-\nu_i)\varepsilon_{zz} - \varphi_i \\
&= 2\nu_i \frac{1}{1-\gamma_i}\left[\left(\gamma_i q_{i-1}^0 - q_i^0\right) + \left(\gamma_i \zeta_{i-1}\varepsilon_{zz} - \zeta_i \varepsilon_{zz}\right)\right] + \hat{E}_i\left(1-\nu_i-2\nu_i^2\right)\varepsilon_{zz} - (1-2\nu_i)\varphi_i \\
&= 2\nu_i \frac{1}{1-\gamma_i}\left(\gamma_i q_{i-1}^0 - q_i^0\right) - (1-2\nu_i)\varphi_i + \left[E_i + 2\nu_i \frac{1}{1-\gamma_i}\left(\gamma_i \zeta_{i-1} - \zeta_i\right)\right]\varepsilon_{zz} .
\end{aligned}
\tag{93}
$$

The resulting expression in Eq. (93) above may subsequently be inserted into the equilibrium equation, Eq. (92), to obtain

$$
\begin{aligned}
&\pi \sum_{i=1}^{n} r_i^2 (1-\gamma_i)\left\{2\nu_i \frac{1}{1-\gamma_i}\left(\gamma_i q_{i-1}^0 - q_i^0\right) - (1-2\nu_i)\varphi_i + \left[E_i + 2\nu_i \frac{1}{1-\gamma_i}\left(\gamma_i \varsigma_{i-1} - \varsigma_i\right)\right]\varepsilon_{zz}\right\} \\
&\qquad = N - KL\varepsilon_{zz} .
\end{aligned}
\tag{94}
$$

From Eq. (94) we may solve for ε_{zz}, which gives

$$
\varepsilon_{zz} = \frac{N + \pi \sum_{i=1}^{n} r_i^2 \left[(1-2\nu_i)(1-\gamma_i)\varphi_i - 2\nu_i\left(\gamma_i q_{i-1}^0 - q_i^0\right)\right]}{KL + \pi \sum_{i=1}^{n} r_i^2 \left[E_i(1-\gamma_i) + 2\nu_i\left(\gamma_i \varsigma_{i-1} - \varsigma_i\right)\right]}
\tag{95}
$$

When the expression for ε_{zz} is determined, the contact pressures can be found from Eq. (90), after which the remaining unknown coefficients A_i and C_i may be determined from Eq. (69), but keeping in mind that φ_i must be replaced by μ_i. Finally, the radial displacement field can be obtained from Eq. (59) and the stresses from Eq. (79).

7 VALIDATION OF THE MULTI-LAYER FORMULAE

7.1 Verification Case

One verification case based on a typical 6-layer offshore pipeline, including a layer of corrosion resistant alloy (CRA) and a thick thermal insulation coating, will be presented. Material characteristics and layer thicknesses have been taken according to an example published by Bouchonneau et al. [2010]. The geometry and material characteristics are presented below in Table 1 along with the applied temperature in each individual layer. The applied internal pressure p_{int} is 220 bar and the external pressure p_{ext} is 15 bar.

Table 1 – Geometry, material characteristics and applied temperatures for the verification case.

Description	Layer number i	r_{i-1} [mm]	r_i [mm]	E_i [GPa]	ν_i [-]	α_i [°C^{-1}]	ΔT_i [°C]
CRA liner	1	172.1	175.1	191	0.29	$1.7 \cdot 10^{-5}$	131.23
CMn steel	2	175.1	194.2	207	0.30	$1.17 \cdot 10^{-5}$	129.02
Epoxy	3	194.2	194.5	3.0	0.40	$5.4 \cdot 10^{-5}$	127.08
Adhesive PP	4	194.5	197.5	1.3	0.40	$1.6 \cdot 10^{-4}$	126.75
Syntactic PP	5	197.5	252.5	1.1	0.32	$5.0 \cdot 10^{-5}$	120.95
Adhesive PP	6	252.5	255.5	1.3	0.40	$1.6 \cdot 10^{-4}$	29.84

7.2 Finite Element Analyses

7.2.1 Element type and Boundary conditions

Finite element analyses (FEA) have been conducted using the commercially available software program Abaqus [2012]. The 8-node brick element C3D8R was used. This is a bi-linear solid element with reduced integration and hourglass control.

The verification case will be analyzed for three separate boundary conditions. With reference to Figure 3 (Section 2.3), the following cases will be studied:

1) Axially fixed (Figure 3 a).
2) Axially free with $K = 0$ and $N = 0$ (Figure 3 b).
3) Spring-mounted with $K = 10^{12}$ N/m and $N = -1.0$ MN (Figure 3 b).

The plane stress condition, where the layers are assumed to slide with no friction, is assumed implicitly verified by the calculations for the plane strain (axially fixed) condition

since the same equations are solved as for plane strain, only introducing a small variation in the stress calculations according to Eqs. (56)-(58).

The Abaqus models were established with kinematic restraints as illustrated on the two cylinder segments in Figure 3 a) and Figure 3 b). In Figure 3 b), the dashed lines indicate a kinematic coupling between a reference point (RP) and the cylinder end surface. In the FE model, the reference point was taken as a master node, and the cylinder end surface was taken as a slave surface. For the case of non-zero axial spring stiffness K and applied axial force N, both the spring force and the axial force were applied at the reference point (RP), as indicated in Figure 3 b).

It was found necessary to model a full cylinder (i.e., the axisymmetry could not be utilized by modeling only a small slice of the cylinder) due to local problems surrounding boundary conditions where multiple master-slave relations, which Abaqus is unable to handle properly, have to be declared. A detailed discussion of why it is reasonable and accurate to model the full cylinder is made by Vedeld and Sollund [2013]. Furthermore, in order to model contact between two adjacent cylinder layers, one of the surfaces would have to be a slave and the other a master surface at the interface between the layers. Thus, at the end cross-section ($z = L$) the interface between the layers would contain two sets of master-slave relations, which is not possible to solve for in Abaqus. Contact modeling is therefore avoided by modeling the six-layer cylinder as a single cylinder with varying material properties and temperatures through the thickness. In other words, the contact surfaces were modeled to be completely coupled, which is reasonable since no axial sliding between the layers occurs in accordance with assumption (viii) (Section 2.1).

7.2.2 Mesh Refinement and Convergence

A convergence study was performed of the finite element solution for increasing mesh refinement. Convergence to 5 significant digits was assumed complete. Full convergence was achieved globally, but the local radial stresses at the interface between cylinder layers did not converge. Only 1 element in the axial direction is necessary for convergence of axial stresses, but 6 elements were chosen in the axial direction to ensure a good aspect ratio. In the hoop direction, convergence was achieved with 180 elements. In the radial direction, overall convergence was achieved with approximately 50 elements over the thickness for both configurations 1 and 2. However, at the interface between layers and at r_i and $r_{o,b}$, , full convergence was not achieved even with 210 elements over the thickness. A small

discontinuity of the radial stresses occurs at the interfaces between layers, and a slight difference between applied pressure and radial stress at the inner radius r_i and outer radius $r_{o,b}$ was observed for all cases considered, similar to the behavior documented by Vedeld and Sollund [2013] for two-layer cylinders. An example of such a discontinuity is illustrated in Figure 7 (Section 7.3).

The full-cylinder analyses included a total of 226800 solid elements, corresponding to approximately 850000 degrees of freedom. The discontinuity at the interface between layers declines with increasing number of elements, but further refinement was considered unnecessary since the discontinuity is obviously unphysical (the contact pressure cannot be different on the two surfaces). Consequently, 226800 elements were used for all boundary conditions, and (minor) discontinuities in radial stresses between layers were disregarded as unphysical. Since the radial stresses at the interface between layers are discontinuous in the finite element solutions, almost regardless of element mesh refinement, it is inefficient to apply FEA for calculation of contact pressures.

7.3 Comparison between FE Results and Results of the Iterative Analytical Method

As described in Section 7.2, three sets of axial boundary conditions were considered for the verification case. The results for the axially free cylinder (with $K = 0$ and $N = 0$) are presented here. The remaining results, obtained for the axially fixed and the spring-mounted boundary conditions, are shown in Appendix A.

Radial stresses calculated by means of FEA and analytically with the iterative method, are compared in Figure 6. As observed from the figure, the analytically derived and FE-derived radial stresses match perfectly.

The discontinuities in radial stresses predicted by FE analyses, as discussed in the preceding section, are illustrated in Figure 7, where a close-up of the radial stress curve at the precise intersection between the CRA liner and the CMn steel (layer 1 and 2 in Table 1) is presented. The relative error in the FE solution at the interface ($r = 0.1751$ m) is 2.1 %.

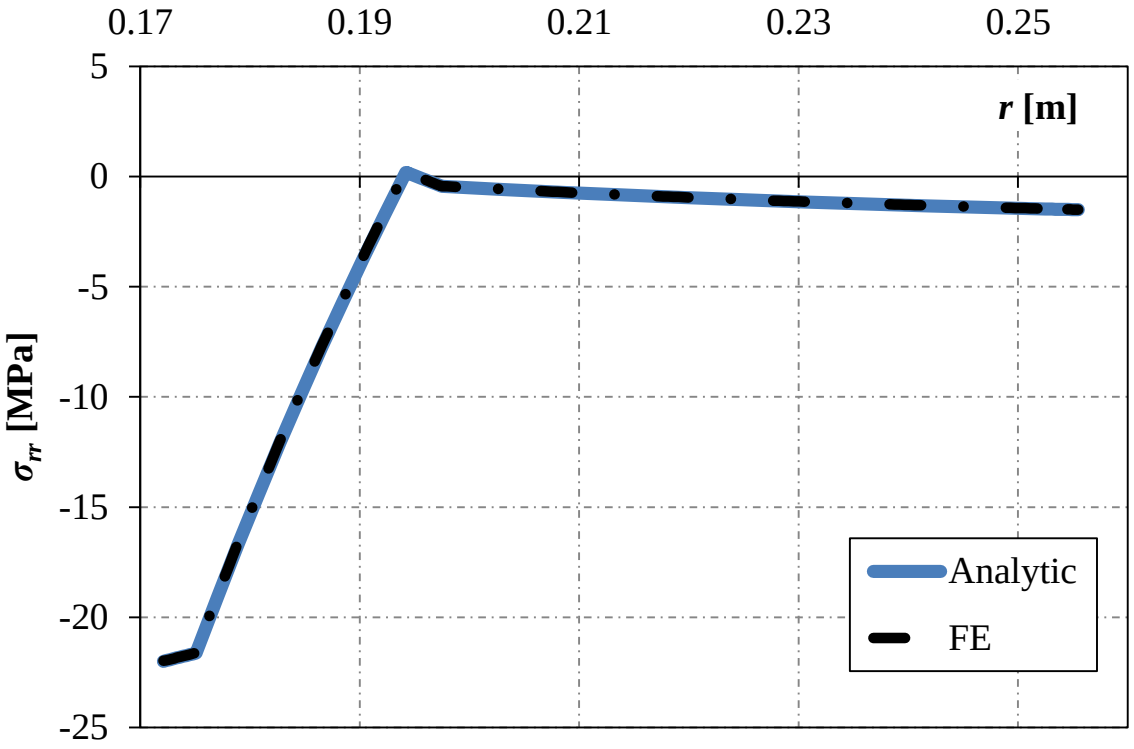

Figure 6 – Radial stresses as a function of *r* for the iterative analytical solution ("Analytic") and the finite element solution ("FE").

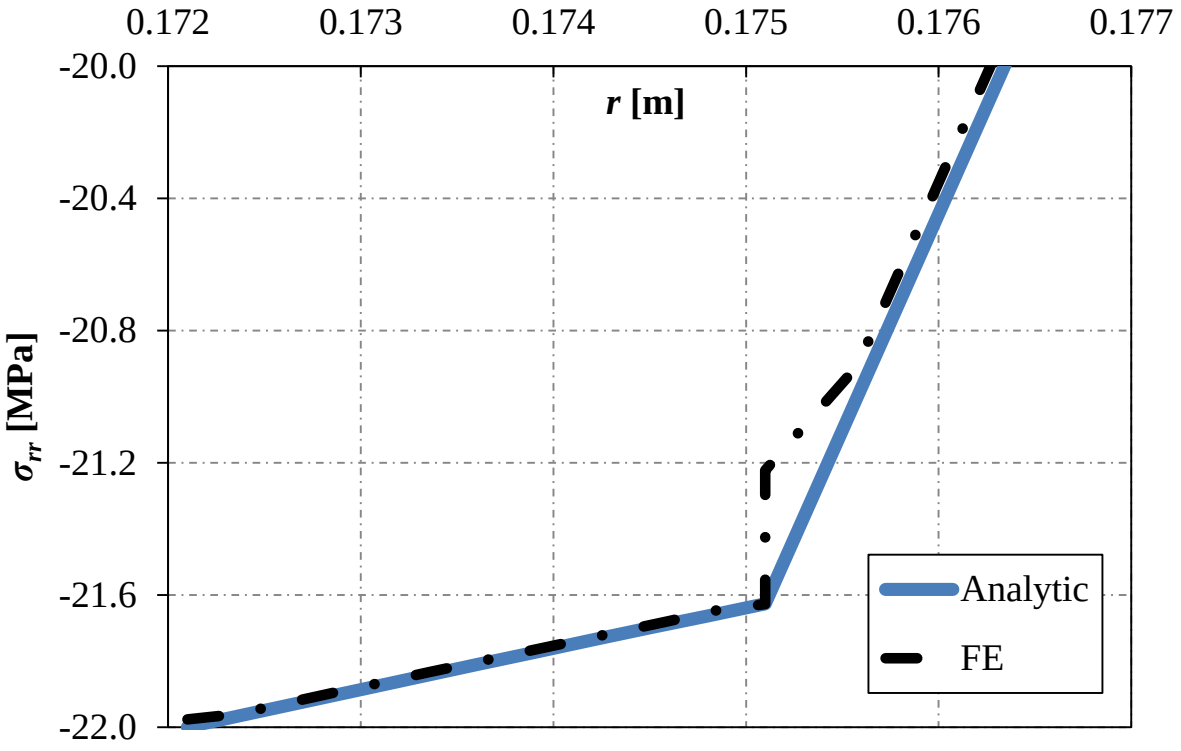

Figure 7 – Close-up view of discontinuity in radial stresses at the interface (*r* = 0.1751 m) between the CRA liner and CMn backing steel.

Hoop stresses are compared in Figure 8. Again it is observed that the iterative analytical solution and the finite element solution match very closely. The solutions are seen to be indistinguishable. No unexpected discontinuities or problems at the interfaces between layers were experienced in the solutions for the hoop stresses.

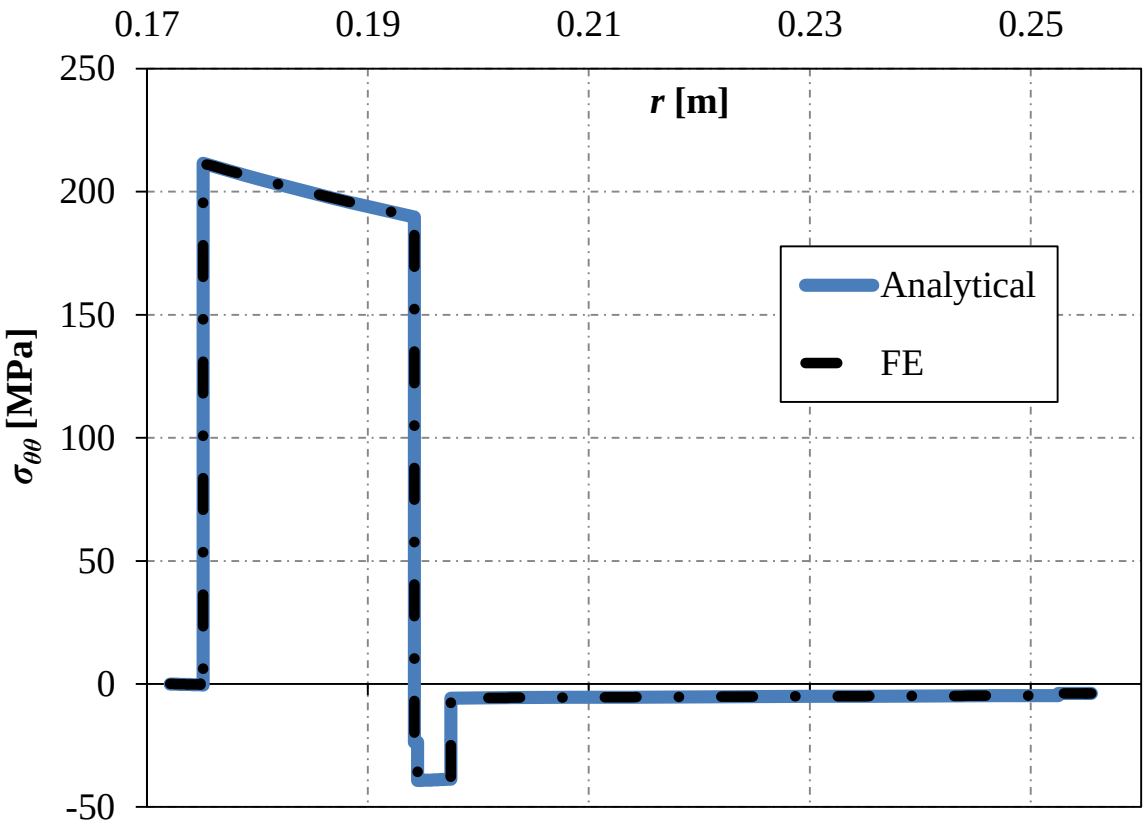

Figure 8 – Hoop stresses as a function of *r* for the iterative analytical solution ("Analytical") and the finite element solution ("FE").

The axial stresses have also been compared. According to the generalized plane strain condition, the axial strains in all layers are constant over the length of the cylinder and as a function of the radial coordinate. Also, the thermal loading is uniform in each individual layer, and the sum of radial and hoop strains is constant (Section 4). Thus, the axial stresses are expected to be constant in each individual layer, but different between layers. The axial stresses in the cylinder, calculated for the verification case as a function of the radial coordinate *r*, are presented in Figure 9. As for the radial and hoop stresses, it is observed that the iterative analytical solution and the finite element solution are indistinguishable.

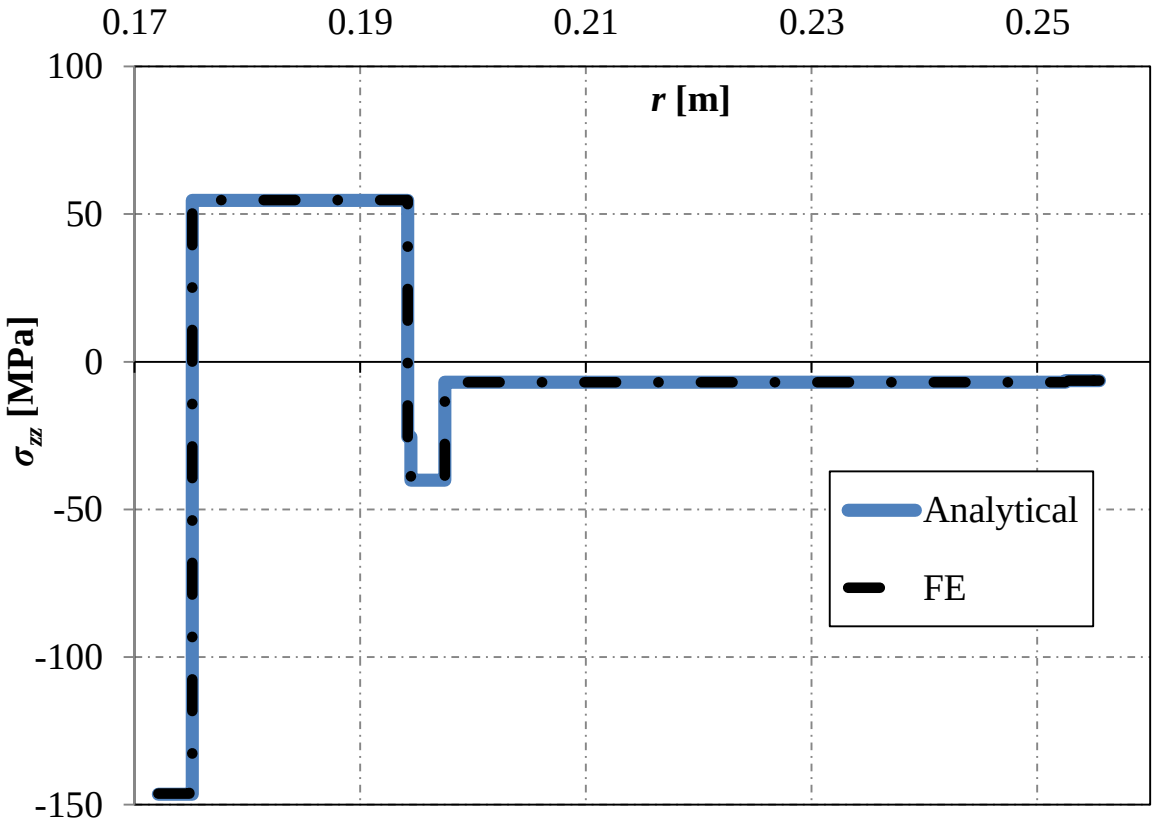

Figure 9 – Axial stresses as a function of *r* for the iterative analytical solution ("Analytical") and the finite element solution ("FE").

The results presented in Figure 6, Figure 8 and Figure 9 show that the iterative analytical solution gives the same results as highly refined and detailed finite element analyses for the axially free boundary condition. The results for the axially fixed and spring-mounted boundary conditions show the same behavior, and the corresponding curves may be found in Appendix A. Based on the comparisons to the finite element analyses, the exact iterative analytical solution presented herein is considered verified.

7.4 Comparison between Results of the Two Analytical Models

The analytical solution based on matrix inversion, described in Section 5, will be compared to the iterative analytical solution presented in Section 6. As investigated in detail by Vedeld and Sollund [2013], each individual layer in a multi-layer cylinder can be interpreted as a single layer cylinder subjected to an axial force, an internal pressure and an external pressure. If the contact pressures and axial stresses are known in each layer, the resulting stress distributions may be calculated according to Lamé's solutions, i.e., according to Eq. (26). Thus, in order to assess whether the two analytical solutions are equivalent, it is

sufficient to compare the contact pressures and axial stresses. The verification case described in Table 1 was used for the comparison, and all three boundary conditions (Section 7.2) were examined. The resulting contact pressures and axial forces are shown below in Table 2. For the iterative analytical method, contact pressures at the inner radius of each layer are indicated by the symbol p_c^{IM} and the axial stresses are indicated by the symbol σ_{zz}^{IM}. For the matrix-based analytical solution, described in Section 5, the corresponding contact pressures and axial stresses are denoted p_c^{MS} and σ_{zz}^{MS}.

Table 2 – Contact pressures and axial stresses for the two analytical solutions.

Layer number i	p_c^{IM} [MPa]	p_c^{MS} [MPa]	σ_{zz}^{IM} [MPa]	σ_{zz}^{MS} [MPa]
Axially free boundary				
1	22.0000	22.0000	-146.3826	-146.3826
2	21.6266	21.6266	54.5872	54.5872
3	-0.182677	-0.182677	-25.4869	-25.4869
4	-0.145918	-0.145918	-40.0604	-40.0604
5	0.448047	0.448047	-6.97980	-6.97980
6	1.472283	1.472283	-6.38640	-6.38640
Axially fixed boundary				
1	22.0000	22.0000	-431.6485	-431.6485
2	21.5777	21.5777	-255.5618	-255.5618
3	-0.197042	-0.197042	-30.18683	-30.18683
4	-0.159445	-0.159445	-42.09194	-42.09194
5	0.438104	0.438164	-8.63341	-8.63341
6	1.46978	1.46978	-8.41738	-8.41738
Spring-mounted boundary				
1	22.0000	22.0000	-366.4441	-366.4441
2	21.5889	21.5889	-184.6698	-184.6698
3	-0.193759	-0.193759	-29.1125	-29.1125
4	-0.156353	-0.156353	-41.6276	-41.6276
5	0.440377	0.440377	-8.25544	-8.25544
6	1.47035	1.47035	-7.95315	-7.95315

From Table 2 it is observed that the correspondence between the two sets of analytical results is perfect. In fact, the solutions were equal with far more digits. However, six significant digits were conveniently considered sufficient to demonstrate the agreement between the results.

8 SUMMARY AND CONCLUSIONS

- The solution presented by Xiang et al. [2006] for a pressurized layered cylinder in plane stress or plane strain has been formally proven by induction.
- The solution presented by Xiang et al. [2006] has been expanded to include temperature expansion in the layers, and new sets of boundary conditions corresponding to generalized plane strain conditions have been included in the solution.
- The new iterative solutions, including new boundary conditions and temperature expansion, have been proven mathematically.
- A physically transparent analytical solution based on matrix inversion has also been developed.
- The iterative methodology has been verified based on both detailed FE analyses and the matrix-based analytical approach.
- The iterative method is computationally efficient and easily implemented. It does not involve matrix inversion or other numerically demanding solution techniques.
- The matrix-based analytical solution is more physically transparent, but also more demanding in terms of computational efficiency.

REFERENCES

Abaqus, v. 6.12, 2012. Dassault Systèmes Simulia Corp., Providence, RI, USA.

Akcay, I.H., Kaynak, I., 2005. Analysis of multilayered composite cylinders under thermal loading. J. Reinf. Plast. Comp. 24, 1169-1179.

ASME B31.8, 2003. Gas transmission and distribution piping systems. American Society of Mechanical Engineers, New York, NY, USA.

Barbezat, G., 2005. Advanced thermal spray technology and coating for lightweight engine blocks for the automotive industry. Surf. Coat. Technol. 200 (5-6), 1990-1993.

Bouchouneu, N., Sauvant-Moynot, V., Choqueuse, D., Grosjean, F., Ponchet, E., Pereux, D., 2010. Experimental testing and modeling of an industrial insulated pipeline for deep sea application. J. Pet. Sci. Eng. 73 (1-2), 1-12.

Braestrup, M.W., Andersen, J.B., Andersen, L.W., Bryndum, M.B., Christensen, J.C., Nielsen, N.J.R., 2005. Design and installation of marine pipelines. Blackwell Science, Oxford, UK.

Cook R.D., Malkus D.S, Plesha M. E., Witt R. J., 2002. Concepts and applications of finite element analysis, fourth ed. John Wiley & Sons, The University of Wisconsin, Madison, WI, USA.

DNV-OS-F101, August 2012. Submarine Pipeline Systems. Offshore Standard. Det Norske Veritas, Høvik, Norway.

Eraslan, A.N., Akis, T., 2006. Plane strain analytical solutions for a functionally graded elastic–plastic pressurized tube. Int. J. Pressure Vessels Piping 83, 635-644.

Fyrileiv, O., Collberg, L., 2005. Influence of pressure in pipeline design: Effective axial force. In: Proceedings of the 24th International Conference on Offshore Mechanics and Arctic Engineering, vol. 3, OMAE 2005-67502, Halkidiki, Greece, June 2005, pp. 629-636.

Horgan, C.O., Chan, A.M., 1999. The pressurized hollow cylinder or disk problem for functionally graded isotropic linearly elastic materials. J. Elasticity 55, 43-59.

Jabbari, M., Sohrabpour, S., Eslami, M.R., 2002. Mechanical and thermal stresses in a functionally graded hollow cylinder due to radially symmetric loads, Int. J. Pressure Vessels Piping 79, 493-497.

Jahed, H., Farshi, B., Karimi, M., 2006. Optimum autofrettage and shrink-fit combination in multi-layer cylinders. ASME J. Pres. Ves. Technol. 128, 196-200.

Kloewer, J., Behrens, R., Lettner, J., 2002. Clad Plates and Pipes in Oil and Gas Production: Applications - Fabrication – Welding. In: Proceedings of Corrosion, April 2002, Denver, CO, USA.

Koizumi, M., 1993. The Concept of FGM. In: Holt, J.B., Koizumi, M., Hirai, T., Munir, Z.A. (eds.). Functionally gradient materials. Ceramic Trans., vol. 34, pp. 3-10. The American Ceramic Society, Westerville, OH, USA.

Lamé, G. and Clapeyron, B., 1831, Mémoire sur l'équilibre intérieur des corps solides homogènes. J. Reine Angew. Math. (Crelle's j.) 7, 145-169.

Liew, K.M., Kitipornchai, S., Zhang, X.Z., Lim, C.W., 2003. Analysis of the thermal stress behaviour of functionally graded hollow circular cylinders. Int. J. Solids Struct. 40, 2355-2380.

Marie, S., 2004. Analytical expression of the thermal stresses in a vessel or pipe with cladding submitted to any thermal restraint. Int. J. Pressure Vessels Piping 81, 303-312.

Noda, N., 1999. Thermal stresses in functionally graded materials. J. Therm. Stresses 22 (4-5), 477-512.

Olsson, J., Grützner, H., 1989. Experiences with a high-alloyed stainless steel under highly corrosive conditions. Mater. Corros. 40 (5), 279-284.

Ootao, Y., Tanigawa, Y., 2006. Transient thermoelastic analysis for a functionally graded hollow cylinder. J. Therm. Stresses 29, 1031-1046.

Palmer, A.C., King, R.A., 2004. Subsea pipeline engineering, second ed. PennWell, Tulsa, OK, USA.

Peng, X.L., Li, X.F., 2010. Thermoelastic analysis of a cylindrical vessel of functionally graded materials. Int. J. Pressure Vessels Piping 87, 203-210.

Reddy, J.N., Chin, C.D., 1998. Thermomechanical analysis of functionally graded cylinders and plates. J. Therm. Stresses 21 (6), 593-626.

Shi, Z., Zhang, T., Xiang, H., 2006. Exact solutions of heterogeneous elastic hollow cylinders. Compos. Struct. 79, 140-147.

Smith, L.M., 2012. Engineering with clad steel, second ed. Technical Series No. 10064, The Nickel Institute, Brussels, Belgium.

Sparks, C.P., 1984. The influence of tension, pressure and weight on pipe and riser deformations and stresses. ASME J. Energy Resour. Technol. 106, 46-54.

Timoshenko, S.P., 1958. Strength of materials, part II, third ed. D. Van Nostrand Company, Princeton, NJ, USA.

Tutuncu, N., 2007. Stresses in thick-walled FGM cylinders with exponentially-varying properties. Eng. Struct. 29, 2032-2035.

Tutuncu, N., Ozturk, M., 2001. Exact solutions for stresses in functionally graded pressure vessels. Composites: Part B 32, 683-686.

Vedeld, K., Osnes, H., Fyrileiv, O., 2012. Analytical expressions for stress distributions in lined pipes: Axial stress and contact pressure interaction. Marine Struct. 26 (1), 1-26.

Vedeld, K., Sollund, H.A., 2013. Explicit analytical solutions for heated, pressurized two-layer cylinders. Research Report in Mechanics, No. 13-x. Mechanics Division, Department of Mathematics, University of Oslo, Norway.

Wilson, W.R.D., Skelton, W.J., 1967. Design of bi-metallic high pressure cylinders. In: Proceedings of the Institution of Mechanical Engineers, vol. 182 (3), Conference Proceedings, September 1967, pp. 1-10.

Yamanouchi, M., Koizumi, M., Hirai, T., Shiota, I. (eds.), 1990. Proceedings of the First International Symposium on Functionally Gradient Materials, FGM ‘90, October 1990, Sendai, Japan. Functionally Gradient Materials Forum and The Society of Non-Traditional Technology, Tokyo, Japan.

Xiang, H., Shi, Z., Zhang, T., 2006. Elastic analyses of heterogeneous hollow cylinders. Mech. Res. Commun. 33, 681-691.

Zhang, Q. Wang, Z.W., Tang, C.Y, Hu, D.P, Xia, L.Z., 2012. Analytical solution of the thermo-mechanical stresses in a multilayered composite pressure vessel considering the influence of closed ends. Int. J. Pressure Vessels Piping 98, 102-110.

APPENDIX A – Comparison between FE Results and Results of the Iterative Analytical Method for the Axially Fixed and the Spring-Mounted Boundary Conditions

The iterative analytical formulae for stress distributions in multi-layer cylinders derived in the present study were verified by comparison to results of detailed FE analyses, as described in Sections 7.2 and 7.3. The multi-layer cylinder configuration described by Table 1 (Section 7.1) was applied for the validation study. The following three boundary conditions were studied:

1. Axially fixed.
2. Axially free with $K = 0$ and $N = 0$.
3. Spring-mounted with $K = 10^{12}$ N/m and $N = -1.0$ MN.

Only results for the axially free boundary condition were shown in Section 7.3. For completeness, all the remaining radial, hoop and axial stress comparisons are displayed in this appendix for the axially restrained and spring mounted boundary conditions.

A.1 Axially Fixed Boundary Condition

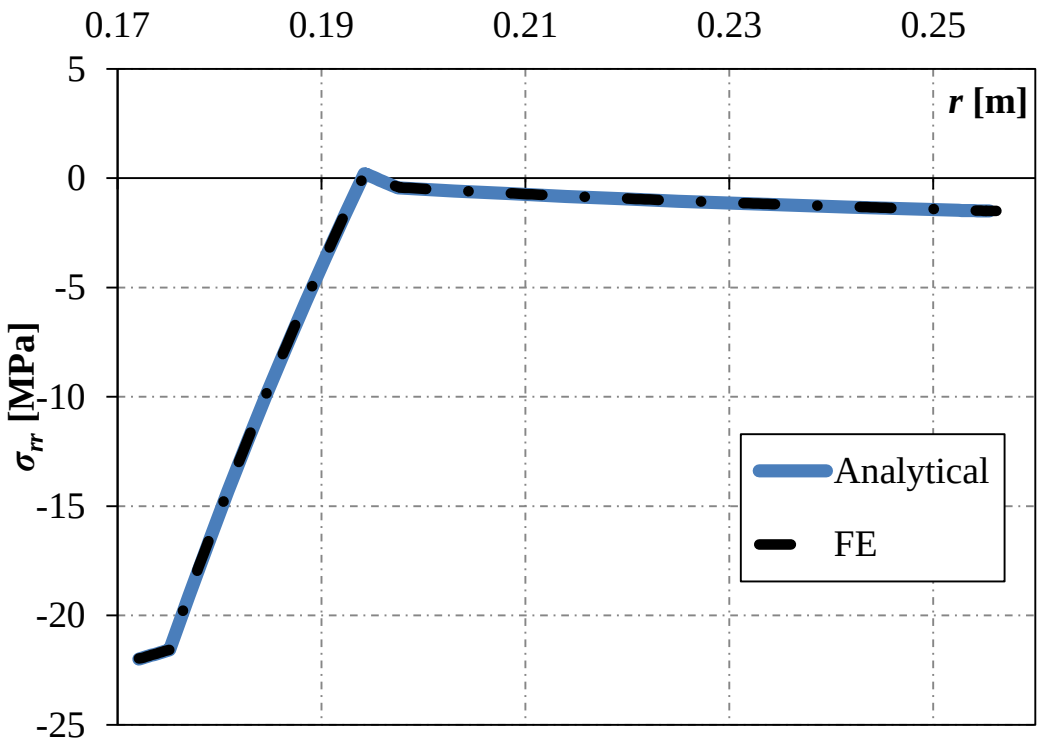

Figure A. 1 - Radial stresses as a function of *r* for the iterative analytical solution ("Analytical") and the finite element solution ("FE") with the axially fixed boundary condition.

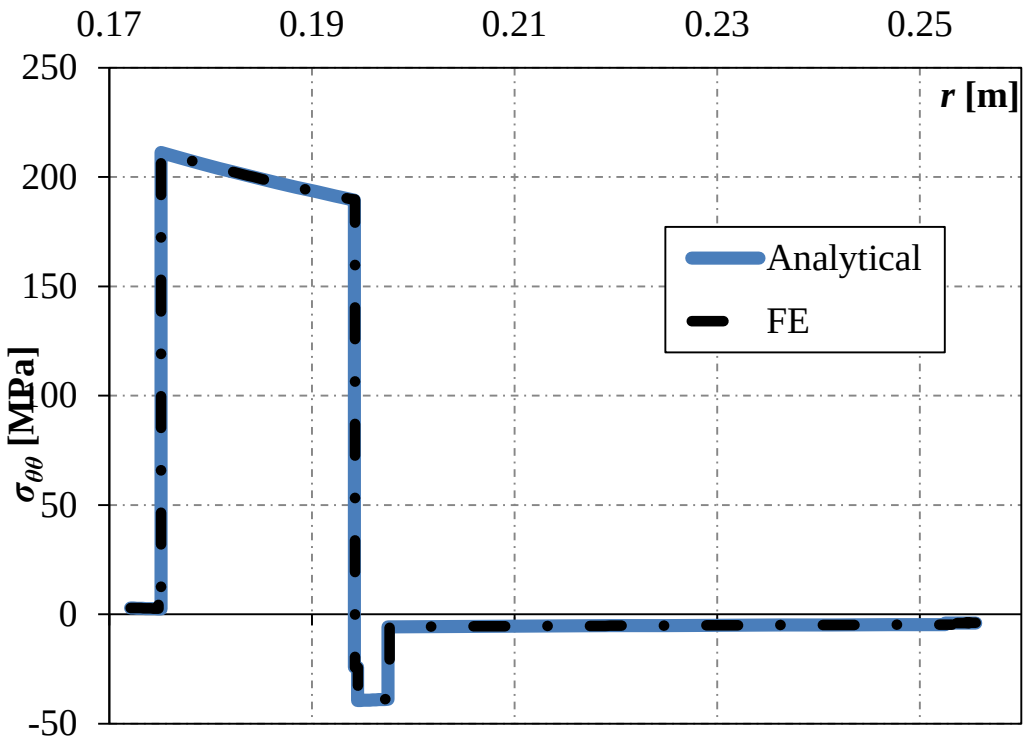

Figure A. 2 - Hoop stresses as a function of *r* for the iterative analytical solution ("Analytical") and the finite element solution ("FE") with the axially fixed boundary condition.

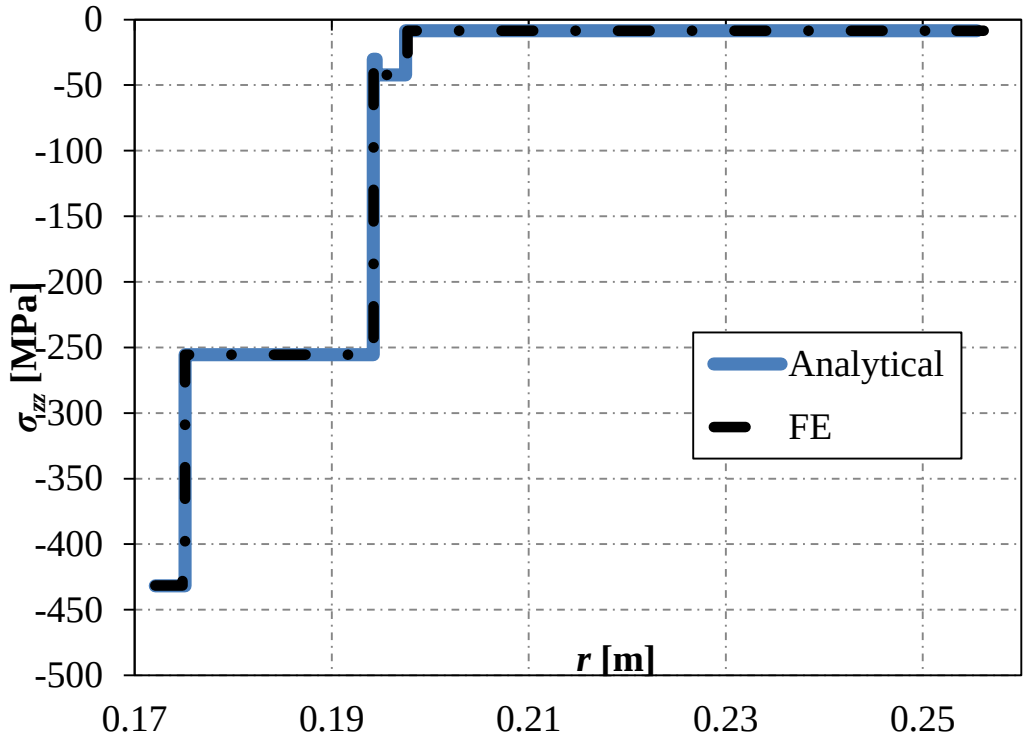

Figure A. 3 - Axial stresses as a function of *r* for the iterative analytical solution ("Analytical") and the finite element solution ("FE") with the axially fixed boundary condition.

A.2 Spring-Mounted Boundary Conditon

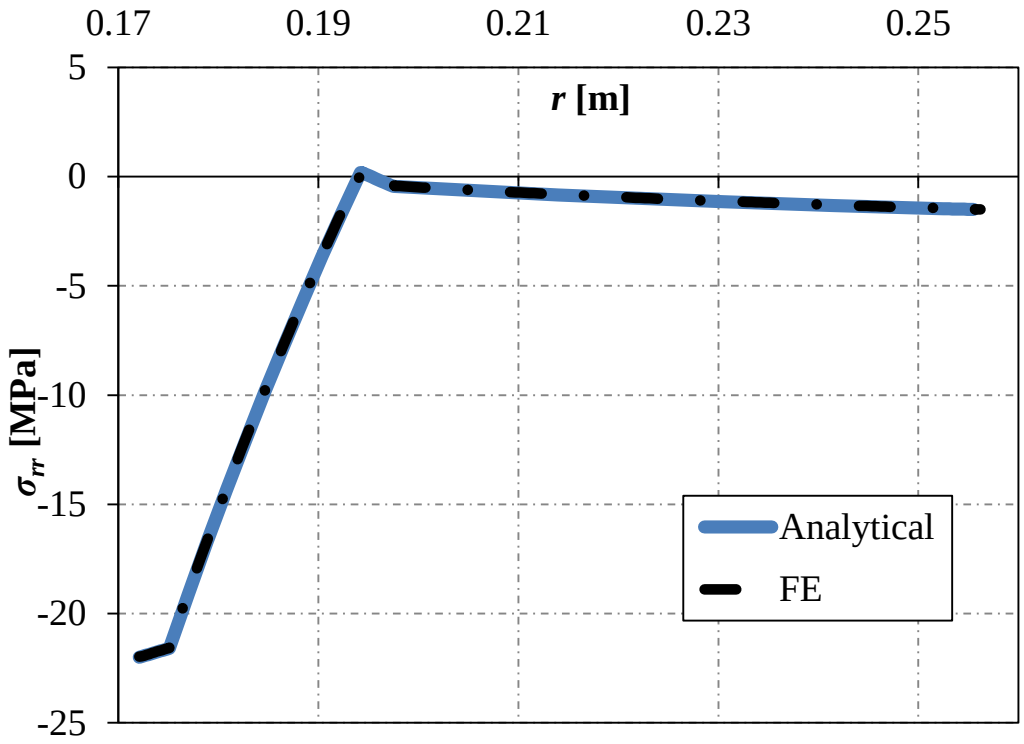

Figure A. 4 - Radial stresses as a function of *r* for the iterative analytical solution ("Analytical") and the finite element solution ("FE") with the spring-mounted boundary condition ($K = 10^{12}$ N/m, N = -1.0 MN).

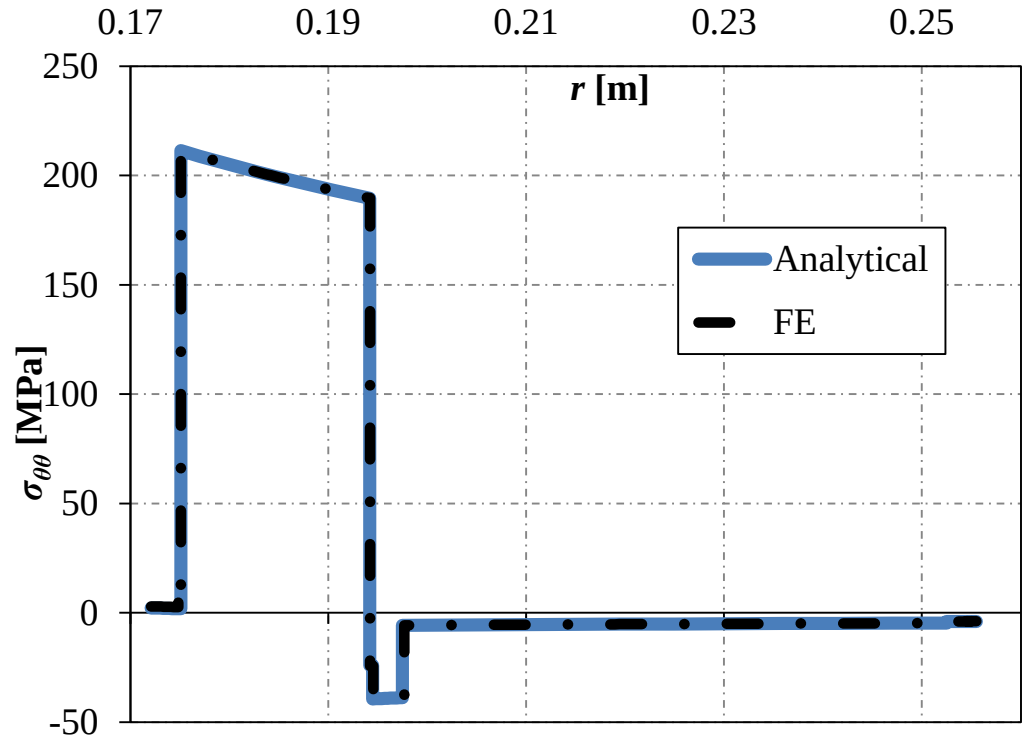

Figure A. 5 - Hoop stresses as a function of *r* for the iterative analytical solution ("Analytical") and the finite element solution ("FE") with the spring-mounted boundary condition ($K = 10^{12}$ N/m, N = -1.0 MN).

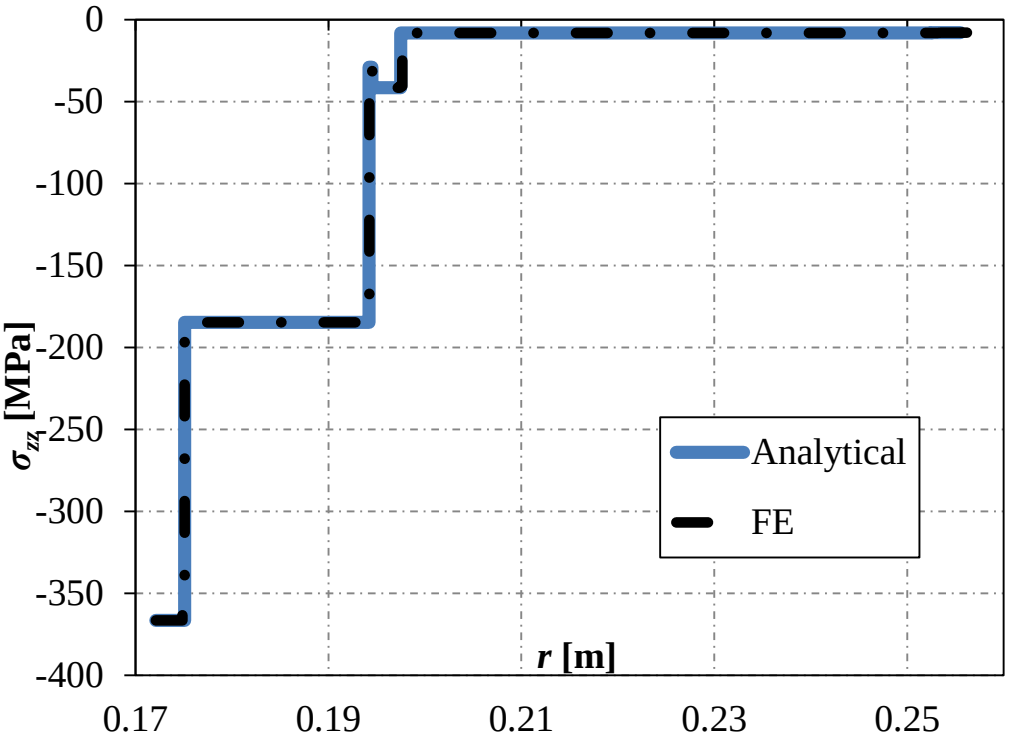

Figure A. 6 - Axial stresses as a function of *r* for the iterative analytical solution ("Analytical") and the finite element solution ("FE") with the spring-mounted boundary condition ($K = 10^{12}$ N/m, $N = -1.0$ MN).